

ADA035611

020-119465-EH
(12)

STUDIES ON THE PENETRATION MECHANICS OF COMPOSITE PLATES

Ref 14

FINAL

R.L. SIERAKOWSKI
C.A. ROSS
L.E. MALVERN
N. CRISTESCU

DECEMBER 31, 1976

U.S. ARMY RESEARCH OFFICE

DAAG29-76-G-0085 ✓

UNIVERSITY OF FLORIDA


DDC
RECEIVED
15 1977
REGISTRATION
C

APPROVED FOR PUBLIC RELEASE;
DISTRIBUTION UNLIMITED.

COPY AVAILABLE TO DDC DOES NOT
PERMIT FULLY LEGIBLE PRODUCTION

TABLE OF CONTENTS

1.	Introduction	
1.1	Background	1
1.2	Research	2
2.	Specimen Fabrication	
2.1	Materials Properties	4
2.2	Composite Materials Preparation	5
3.	Experimental Tests	
3.1	Introduction	9
3.2	Fiber Pullout Tests	9
3.3	Flat Beam Bending Tests	9
3.4	Impact Tests	10
3.5	Blast Loading Tests	13
4.	Discussion of Experimental Results	
4.1	Introduction	15
4.2	Fiber Pull Out Tests	15
4.3	Static and Dynamic Flat Beam Tests	16
4.4	Impact Tests	17
4.5	Blast Loading	21
5.	Analysis	
5.1	Plane Stress Plate Bending	25
5.1.1	Introduction	25
5.1.2	Impact Analysis	27
5.1.3	Blast Analysis	32
5.2	Cylindrical Bending of 0°-90° Laminated Plates with Orthotropic Laminae	36
5.2.1	Introduction	36
5.2.2	Static Cylindrical Bending Analysis for 0°-90° Laminated Plates with Orthotropic Laminae	36
5.2.3	Examples of Estimates for Glass-Epoxy Plates	39
6.	Concluding Remarks	41

BY 	
DISTRIBUTION/AVAILABILITY CODES	UNCLASSIFIED
Dist. ATAL Ref. # SPECIAL	Justification
	Excluded from automatic downgrading and declassification
	DATE OF REVIEW
	REVIEWED BY

1. INTRODUCTION

1.1 Background

The use of multiphase materials for applications to a wide variety of structural systems has been demonstrated during recent years as reported on, for example, in reference [1]. For Army related applications, the uses of composite materials as structural components in aircraft and ground vehicles as well as energy absorbing materials for armor protective systems are of primary importance. In such applications, an understanding of the response characteristics of composite materials under dynamic loading is needed.

Some early experiments related to studying the terminal ballistics problem of fiberglass-reinforced plastics are reported in [2]. Results obtained in [2] indicated a linear relation to exist between impact energy of the projectile and energy loss in penetrating plates of differing densities as well as thicknesses. Some further experiments related to examining the impact resistance of fiberglass type plates reinforced by wire sheet have been examined in [3]. These results have shown an improvement in the impact resistance of such plates. Some later studies on a variety of fibrous composite plates were reported on in [4]. A comparison of results based upon an areal density merit rating system has indicated a favorable energy absorption potential for fiberglass composites. In addition, the transparent plate properties have allowed for the observation of sequential delamination patterns occurring during the impact process which were found to be dependent upon the specific ply orientations. These observations have led to the formulation of a so-called generator strip model for explaining the sequential development of the delaminations obtained for a variety of ply orientations. [5]. Studies of the large deflection of opaque backup composite materials for potential use with front faced ceramic type materials under impact loading have been examined in reference [6]. The composites studied such as graphite-epoxy were selected on the basis of energy absorption potential as generated through plastic deformation or interlaminar shear failure. Test results indicated that for such applications composites having a fiber with a low density, high tensile strength and high stiffness, and low interfacial bond strength with the matrix are important. Further penetration studies on impacted graphite-epoxy and boron-epoxy panels consisting of seven and twelve laminas under an initial prestress have been examined in reference [7]. Such studies have focused principally on data collection for predicting ballistic damage and retained residual strength after perforation of the panels. A variety of failure patterns for different combinations of prestress and ply orientations have been presented. Some additional studies on dynamically loaded graphite-epoxy panels tested in a shock tube facility have been discussed in reference [8]. Several interesting tensile composite failure modes have been observed for the specimens tested.

Ballistic tests run on woven and knitted type textile fabrics molded into composite panels have been reported on in reference [9]. A variety of failure modes have been observed, each of which is dependent upon the type of fibers and specific weave patterns used within the given matrix. The energy absorption of such materials is considered to depend upon penetration strength of the material as well as the ability of the structure to propagate large strains within the target medium. Some recent tests on fabric type composites examining the effect of glass-resin interface strength during Charpy impact loading have been reported in reference [10]. Both the initiation and propagation energies are reported. Further, a critical impact energy is introduced with the dominant energy absorption mechanism below this value stated to be delamination.

Slower speed dynamic tests of the Charpy and Izod impact type have also been used as diagnostic and screening tests for predicting composite failure modes [11-14]. Some early work studying the fracture behavior of unidirectional composites with various filament types containing boron, graphite, glass, and Kevlar were reported in reference [11]. This study indicated the importance of fiber properties in improving the impact resistance of composites and suggested that delamination was a major energy absorbing mechanism. The importance of the laminate orientation in energy absorption has been demonstrated in the impact drop tests described in reference [12]. Some further results on differences in specimen failure are described in reference [13] for graphite-epoxy cantilever beams subjected to impact loading. For these tests a pendulum was used as the impactor on three separate fiber layup configurations with failure observed to occur for the alternating 0/90 ply composites on the tension side between the plies. The consideration of hybrid type composites, that is several fiber types in an epoxy matrix has been studied in reference [14]. Results from this study for unidirectional and angle ply laminates indicate that improved impact resistance can be obtained by combining different fiber types within a given matrix.

1.2 Research

The present studies have been directed toward providing information on material characterization related to the terminal ballistics problem and specifically the energy absorbing mechanisms involved during structural impact. In particular, a series of diagnostic type tests have been used to examine the dominant mechanisms leading up to plate perforation. Two specific types of composite systems were selected for initial study, these being representative ductile and brittle fibers incorporated within an essentially elastic matrix. For the ductile fiber, static pull-out tests on single and multiple fibers embedded in the matrix material and sandwiched between laminas of the composite were studied to examine the influence of fiber-fiber and fiber-lamina interaction. Bending coupon samples fabricated from both the

ductile and brittle fibers have been tested both statically and dynamically. The dynamic tests included stress concentrations, introduced into the specimens, by drilling holes through the top lamina equal in diameter to the impacting penetrator. Additional experiments were then conducted on several size plate configurations with varying lamina orientations and stacking sequences to examine the energy absorption characteristic of such systems. Some analytical results associated with a dynamic elastic response code known as DEPROP are included for comparison with experimental data.

Some simple elastic analyses were also made for cylindrical bending of laminated plates with orthotropic laminae having unequal moduli in tension and compression. The purpose of these calculations was to obtain an idea of the order of magnitude of the asymmetry of the flexural shear stress distribution through the thickness that is caused by unequal moduli, and in particular the location of the maximum shear stress.

2. SPECIMEN FABRICATION

2.1 Materials Properties

Composite specimens, that is those consisting of fibers embedded in a matrix material, can be of the following general types: (a) A resin matrix with a brittle or ductile fiber, or, (b) A metal matrix having a brittle or ductile fiber. For the present work, composites of the resin matrix type with some degree of matrix transparency were selected for study. This was based upon the prior experience of the investigators in producing controlled specimens of varying volume fraction and fiber orientation which when tested could be examined for failure after the test. The specific materials selected for fabrication, while not considered conventionally of the high performance type, were selected for their handling quantities, ease of fabrication by any of several documented fabrication methods, availability and previously observed failure patterns occurring within such material systems. For the major part of the testing program structural composite laminates fabricated from the basic raw materials were used using 50 per cent matrix by weight, although prepreg and fabric weave types were also tested. The impregnated specimens were fabricated at the University of Florida using a resin impregnation procedure with stainless steel or E-glass fibers, while the latter specimens were fabricated elsewhere. Some of the typical properties associated with these materials are included below.

Fiber Types Used

Owens Corning Fiberglass ECD-450-1/0-4
ECG-150-1/0-4 All glass types tested
ECG-801AB-1167

Density	2550 Kg/m ³ [.092 lb/in ³]
Tensile Modulus	72,400 MN/m ² [10.5 x 10 ⁶ lb/in ²]
Filament Strength	2930 MN/m ² [425,000 lb/in ²]

Type 304 Stainless Steel

Density	7850 Kg/m ³ [.283 lb/in ³]
Tensile Modulus	193,000 MN/m ² [28.0 x 10 ⁶ lb/in ²]
Filament Strength	565 MN/m ² [82,000 lb/in ²]

Matrix Used

Shell Epon 828, Curing Agent 400 (10:1)

Density	1170-1230 Kg/m ³ [.042-.44 lb/in ³]
Tensile Modulus	3700-4600 MN/m ² [.54-.66 x 10 ⁶ lb/in ²]
Tensile Strength	62-76 MN/m ² [9000-11,000 lb/in ²]

Prepreg Tapes

Scotchply Type 1002

Density	1800 Kg/m ³ [.065 lb/in ³]
Tensile Modulus	39,200 MN/m ² [5.7 x 10 ⁶ lb/in ²]
Tensile Strength	1100 MN/m ² [160,000 lb/in ²]

2.2 Composite Materials Preparation

Fabrication of the two composite types formed from the constituent materials (steel epoxy and glass epoxy) was accomplished using the winding assembly shown in Fig. 1. Several different wire sizes were used in fabricating the steel composite specimens (1×10^{-4} m, 2×10^{-4} m, and 4×10^{-4} m) with primary attention focused on the largest wire size. Two mandrel sizes were also used in specimen fabrication (.15 m square and .31 m square) for all of the specimens fabricated, with 6061-T6 aluminum used as the mandrel material. The mandrels were sprayed in all cases with Teflon release agent to ensure easy removal of the fabricated plates from the mandrel assembly.

In fabricating the controlled volume fraction and accurately spaced three layer stainless steel wire specimens, for the pull out tests, additional care was introduced during fabrication. For example, the middle layers of such specimens could consist of a single wire, three wires, or a complete layer. The following fabrication procedure described is for a three wire middle layer composite surrounded by two complete layers. Fabrication consisted of placing the 6061-T6 aluminum mandrel into the special jig fixture as shown in Fig. 1. Lathe speed and cross feed were adjusted to insure controlled fiber spacing with tension in the wire maintained by using a pre-set minimum load on the wire as the wire was unwound from the spool. Interlamina spacing was controlled by placing metal shim shock spacers located at the ends of the mandrel assembly. For the single and three middle layers, a set of tightening posts was clamped to one side of the plate assembly in order to maintain a minimum fiber tension and to ensure proper inter fiber spacing. Once positioned, the mid surface wires were clamped along the plate edges and sealed with Devcon compound to the mandrel frame with bar clamps and the tightening posts removed. The final continuous layer of wire was then wound onto the mandrel using end spacers located at the mandrel boundaries and of equal thickness to those used for the bottom and middle layers. A photograph of a three wire middle surface specimen during preparation is shown in Fig. 2. After the skeletal wire lamina frame has been wound on the mandrel assembly, and degreased using trichloroethylene, a silicon rubber sealing compound was used as a dam to seal the edges of the mandrel assembly and the preheated, air evacuated epoxy, was poured into the completed mold. The complete assembly was then cured in an oven at 150°F for two hours. The

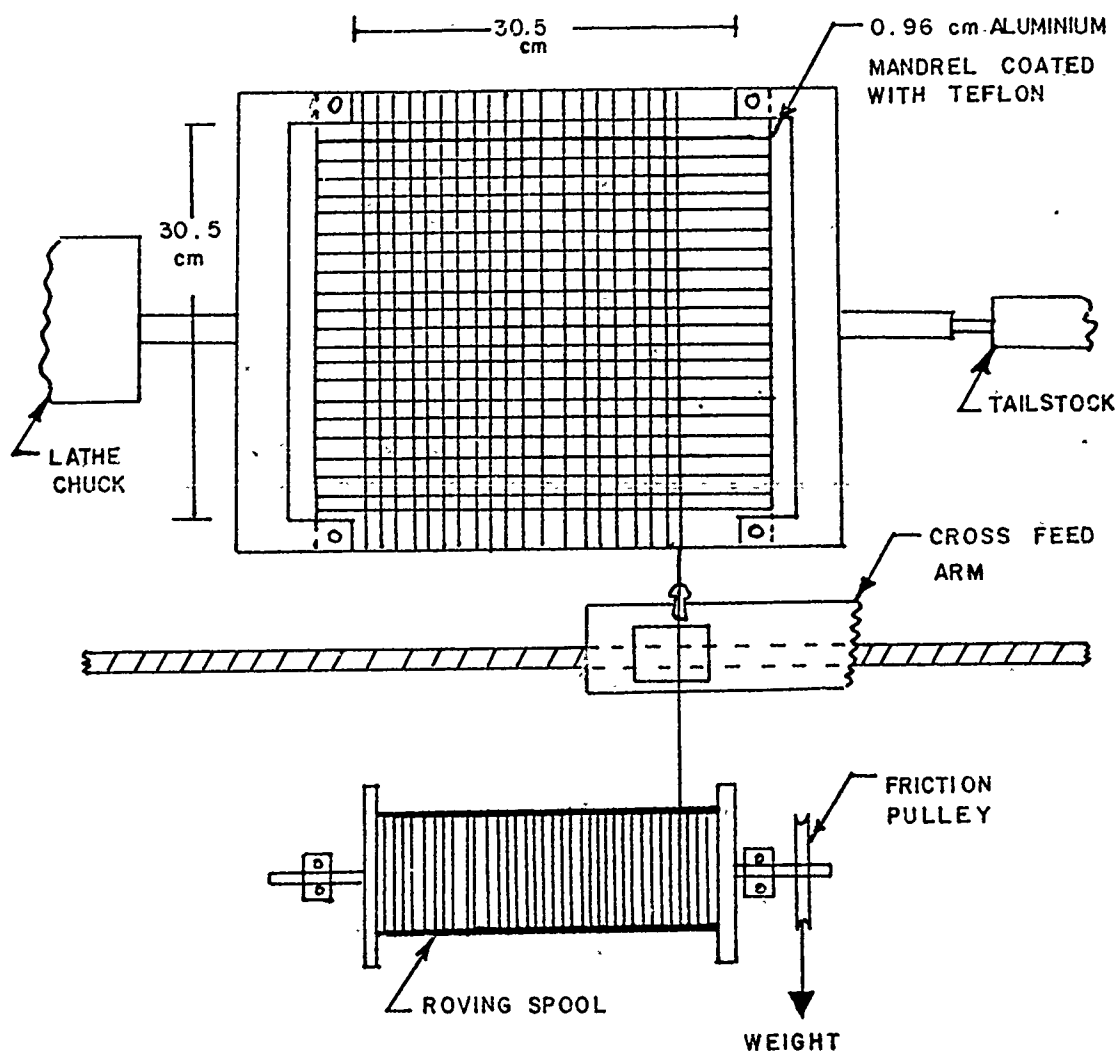


Fig.1 Winding Apparatus for Orthotropic Plates

furnace was then turned off and the specimen allowed to furnace cool over a nominal twenty-four hour period.

For both the multilayer beam and plate specimens tested consisting of steel and E-glass fibers, the following procedure was used. The fibers were wound onto the aluminum plate in the lathe assembly shown in Fig. 1 with fiber spacing adjusted by a cross feed arm, and lamina spacing ensured by using shim stock placed along the edges of the mandrel. Nominal interlamina

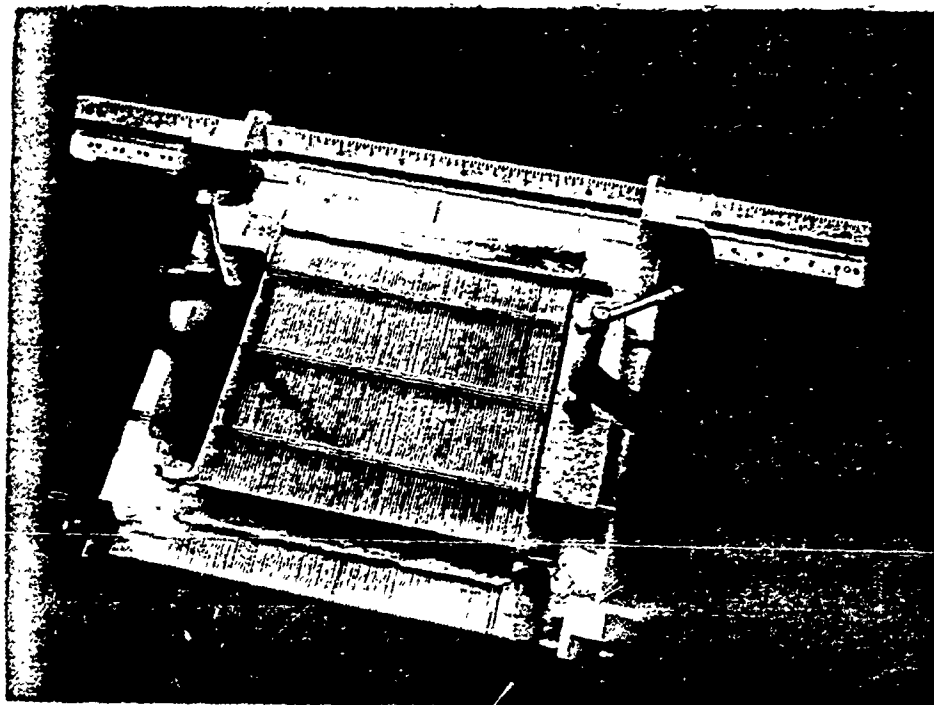


Fig.2 Fabrication of Three Wire Stainless Steel Specimens

spacing was $.18 \times 10^{-2}$ m and interfiber spacing was $.04 \times 10^{-2}$ m. For the twelve strand roving fiberglass specimens a noticeable spreading of the fiberglass was evident during the winding process such that an observable gap space between individual rovings was not apparent but rather a continuous layer. After each layer of fibers had been wound, the next ply was wound until the desired number of unidirectional plies within a given lamina were obtained. The mandrel assembly would then be rotated 90° in its plane and the next lamina developed until a fifteen ply laminate was constructed. For the steel specimens, the edges of the specimen were sealed with a rubber sealing compound, the air evacuated matrix was then poured carefully into the mold assembly and adjustable platens placed over the top of the specimen to ensure a controlled thickness specimen. A slight modification of the procedure was used for producing the fiberglass specimens. After each layer of fiberglass was wound onto the mandrel the fiberglass was impregnated with the matrix material by brushing the preheated air-evacuated epoxy onto the individual layer. This was done until the desired orthotropic arrangement was developed, total number of plies 15, whereupon the specimen was sealed along the edges and the end platens fixed to the mandrel to control the specimen thickness, nominally 6.4×10^{-3} m. This fabrication arrangement produced uniform samples for the test program from which the tensile, beam, and smaller plate

specimens were cut. In all cases two platelike specimens were prepared from each casting procedure with the two larger plates (.31 m square) producing eight of the smaller plates (.15 m square) used in the testing program. Table I summarizing the plate configurations fabricated is found below. The layering sequence number represents the number of layers in the lamina reading front to back. As an example a 5-5-5 plate would have 3 laminae with 5 layers in each lamina.

TABLE I

Layering Arrangements in the Plates Tested

Code	Layering Sequence	Number of Interlaminar Planes
b	1-1-1-1-1-1-1-1-1-1-1-1-1-1-1-1	14
c	1-2-3-4-5	4
d	2-1-2-1-2-1-2-1-2-1	9
e	2-2-2-2-2-2-2-1	7
g	3-1-3-1-3-1-3	6
h	3-2-3-2-3-2	5
i	3-3-3-3-3	4
j	3-4-3-4-1	4
k	3-5-3-4	3
l	4-1-4-1-4-1	5
m	4-4-4-3	3
n	5-1-5-1-3	4
r	5-4-3-2-1	4
o	5-5-5	2
p	8-7	1

Other orthotropic plates, produced from prepreg Scotchply 1002 tape, and fabricated into some of the tabulated configurations shown above using a standard autoclave fabrication procedure, were received from the manufacturer for testing (types b,i,o). In addition, an impregnated fiberglass cloth roving fabricated by a vacuum bagging procedure was obtained and tested.

3. EXPERIMENTAL TESTS

3.1 Introduction

Previous experimental work by the authors [4] showed penetration resistance, based on areal density, of glass-epoxy plates to be better than that exhibited by steel plates and assorted composite materials plates. In addition the glass-epoxy plates showed a delamination pattern which appeared to be related not only to impact velocity but also related to the geometric properties and ply arrangement of the plate. Further examination [5] of these impacted glass-epoxy plates revealed rather regular delamination patterns, and it was concluded that the major energy absorption mechanism for this type of plate was that of interlaminar delamination. Based on these observations and conclusions an experimental program was established to study the delamination process and failure mechanisms for both glass-epoxy (brittle matrix and fiber) and steel-epoxy (brittle matrix, ductile fiber) systems.

Fiber pullout tests, beam bending, plate impact, and blast loading tests of plates, were conducted for various ply and fiber arrangements. These tests will be discussed in some detail in the following sections.

3.2 Fiber Pullout Tests

Quasi-static or static pullout tests were performed on various kinds of steel-epoxy specimens as shown in Table II. (In addition the types of specimens used in the impact are included in this table.) Fiber pullout was performed using a Tinius Olsen Universal Testing Machine. Cross-head speed was varied in order to study the loading rate influence on filament stretching and debonding during pullout.

3.3 Flat Beam Bending Tests

Bending specimens in the form of flat beams [or strip plates] 2.54 cm wide by 15.24 cm long and nominally .6 cm deep were obtained by cutting six strips from each 15.24-cm-square plate. These specimens were loaded by simply supporting the ends and applying the loading at the midpoint of the beam using the Tinius Olsen testing machine as shown in Figure 3. For the three-lamina steel-epoxy specimens, predrilled holes cutting a single lamina were also studies to examine crack initiation, propagation, and potential generator strip development. The careful machining required to produce such controlled specimens was found to be difficult with the fiberglass specimens due to the ability to control single lamina cutting actions. These tests were conducted as diagnostic tests to examine composite failure mechanisms for later reference to the dynamic tests performed on plate type specimens. The load and deflections were recorded electronically on a strip chart using the load cell in the machine head and a portable deflectometer

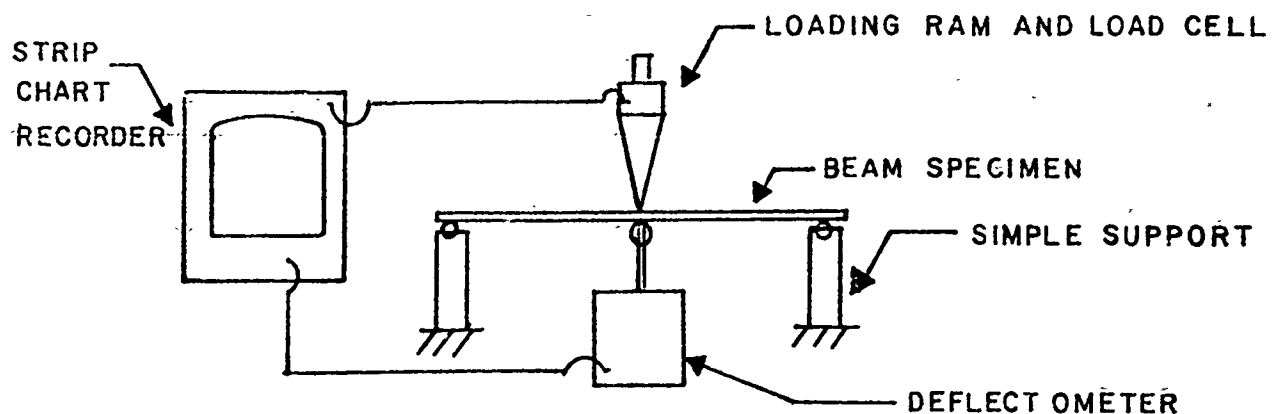


Figure 3. Beam Bending Test Arrangement

placed at the midpoint of the beam. Very close visual observations were made to determine the load causing initial delamination and extent of delamination.

3.4 Impact Tests

Impact tests were performed on beam specimens (4" x 1" x 1/4") and on 15.24 cm (6") square glass-epoxy plates using blunt-ended circular cylindrical projectiles at velocities below the critical penetration velocities. The projectile remained undeformed in all impact tests. The sides of the plates were held fixed at the edges by picture-frame type clamps. The center of the plate was impacted normally by projectiles fired from an air gun system described in Reference [4] and shown schematically in Figure 4.

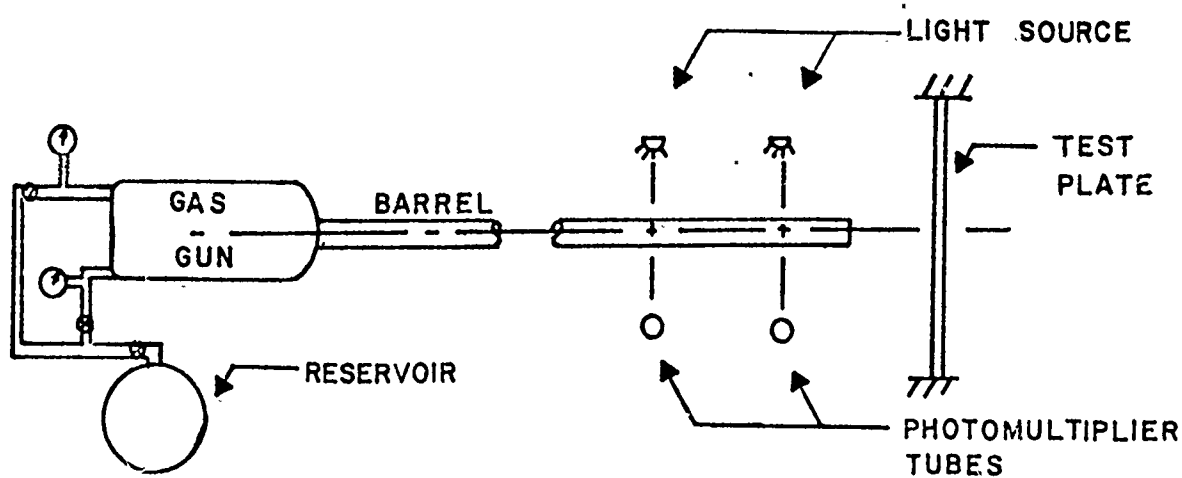


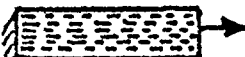






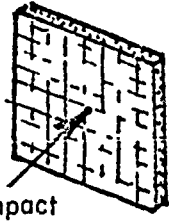


Figure 4. Schematic of Gas Gun and Related Equipment.

TABLE II

Specimen Type and Kind of Test for Filamentary Composites Materials

Specimen Type	Kind of Test	
	Static	Dynamic
a) Steel Fiber only	 Tension	
b) Single Steel fiber in matrix	 Fibre pull-out	
c) Multiple fibers in matrix; steel fibers	 Single fibre pull-out	
d) Single fiber sandwiched between two multifilament lamina in a matrix; steel and glass fiber	 Fibre pull-out	 Impact
e) Three fibers sandwiched between two multifilament lamina in a matrix; steel fiber	 Single fibre pull-out	 Impact
f) Multiple fibers sandwiched between two multifilament lamina in a matrix; steel and glass fiber	 Single fibre pull-out	 Impact
g) Impact tests on 0°-90° cross-plied multifilament in a matrix plate; steel-epoxy and glass epoxy		 Impact

Impact velocities were measured by use of two light beams and photomultiplier tubes spaced 10.16 cm (4") apart at the end of the barrel. The output of the photomultiplier tubes was displayed on a storage oscilloscope and the interruptions in output caused by passage of the projectiles produced a step in the voltage output. The time difference between these steps divided into the spacing of the light beams then gives the projectile velocity. The projectile velocity was varied by changes in chamber pressure of the gas gun. In order that effects of plate size could be investigated, plates 30.48 cm (12") square were tested in the same manner as the 15.24 cm square plates. Also a circular plate holder was used to produce an edge effect similar to that of a circular plate. Schematics of all three types of holders are shown in Figure 5.

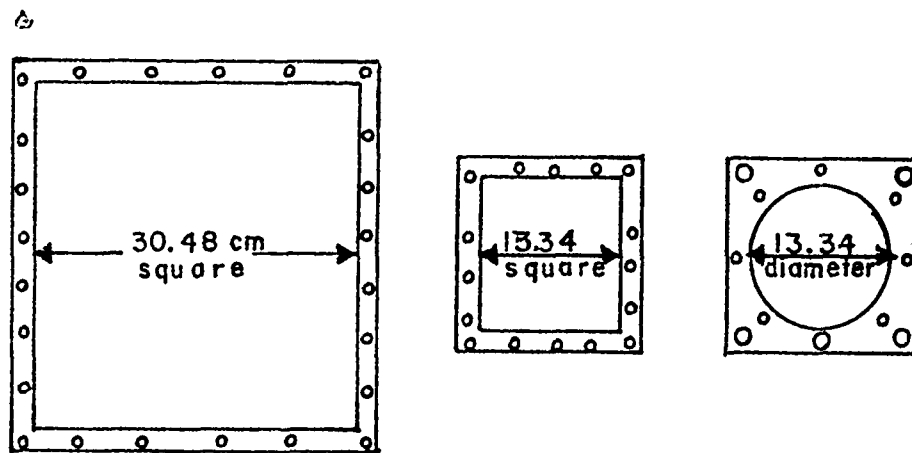


Figure 5. Schematic of Various Types of Plate Holders

This type of test was restricted mainly to the glass-epoxy plates; however, a few steel-epoxy plates were tested. Impact velocities were usually held below the penetration velocity of the plate. Measurements of post impact velocities were attempted but due to splitting of the back lamina of the plate the projectile path was very unpredictable and measured residual velocities were not reliable.

Low velocity repeated impact tests were performed on both steel-epoxy and glass epoxy plates with velocities ranging between 5 and 72 m/sec. The test specimen chosen for this type test was that of a 2.54 cm (1.0") wide and 7.62 cm (3.0") long specimen fixed at either end and backed by a steel plate except near the impact point. The test specimen is shown schematically in Figure 6.

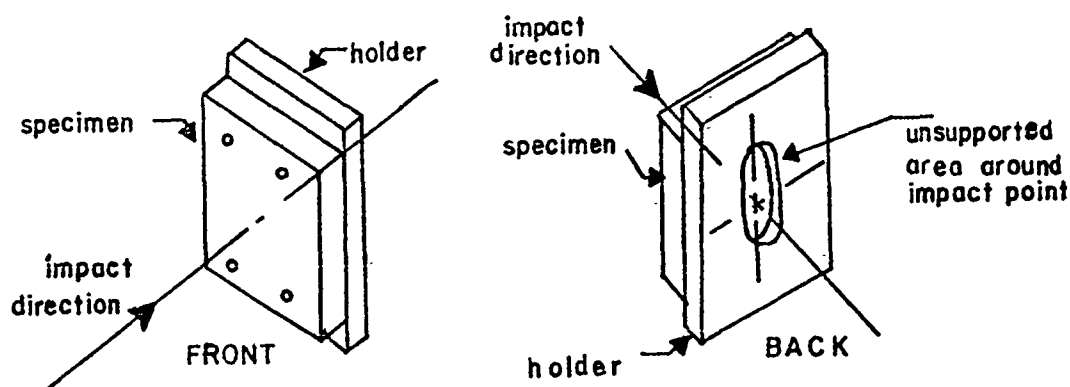


Figure 6. Schematic of Specimen and Specimen Holder for Repeated Impact Tests

In order to observe the sequential delamination mechanism some of the specimens were drilled on both sides such that only the middle lamina remained, as shown for the steel epoxy specimen of Figure 7.

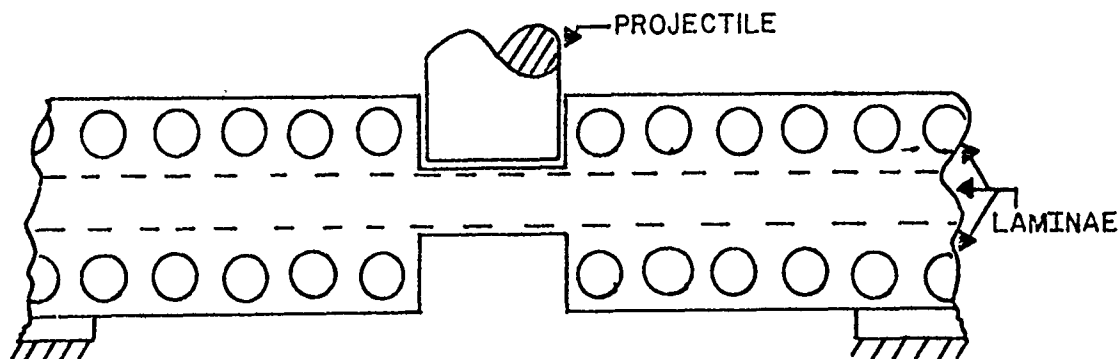


Figure 7. Schematic of Middle Lamina Impact Specimen

3.5 Blast Loading Tests.

Blast loading of 30.48 cm (12.0") square glass-epoxy panels of various ply orientations was performed in cooperation with the Air Force Armament Laboratory and the Test and Evaluation Experimental Facility at Eglin AFB, Fla, Reference [15]. For this test a fuel-air explosion was directed onto the plates to simulate a blast load. A planar blast wave is generated in a

plastic bag, shown schematically in Figure 8, by mixing .91 kg (2 lbs.) of MAPP gas with air in the bag and detonating the mixture at one end of the bag. Upon detonation a plane wave moves away from the detonating charge at a constant velocity and pressure and impinges on the plate at the opposite end. The maximum peak reflected pressure applied to the plate is varied by varying the distance D between the bag and plate. Maximum reflected pressure of .72 to .18 MPa (800 to 200 psi) with positive pressure phases lasting between one and two milliseconds are obtainable using this device. The plates were held fixed by drilling and bolting of all sides reducing the overall plate area to 25.4 cm (10") square. Friction devices were used to hold the sides of the plates and bolts were torqued to prescribed levels in order to prevent plate slippage. Plates containing three, five and fifteen laminae were tested at various peak blast loads.

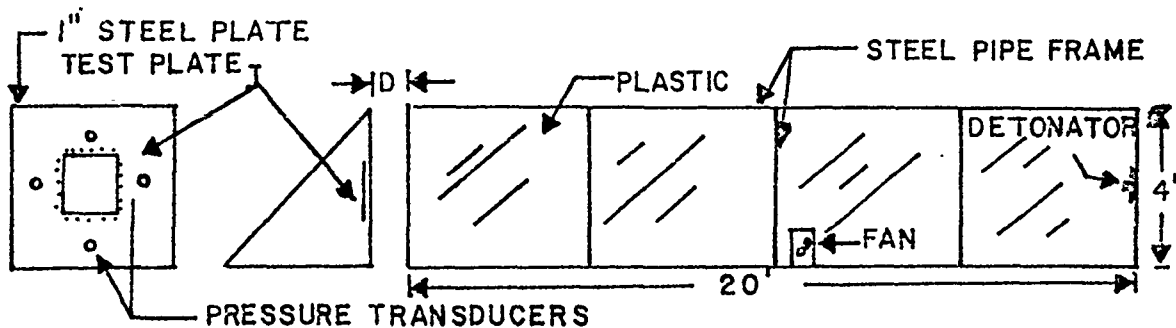


Figure 8. Fuel Air Explosion Loading Device

4. DISCUSSION OF EXPERIMENTAL RESULTS

4.1 Introduction

As mentioned in Section III, a series of fiber pullout, beam bending, plate impact and blast loading tests were conducted on the principal composite material types reported herein. A summary of this work, as reported on in greater detail in references [5, 16-19] is included below.

4.2 Fiber Pull Out Tests

In order to assess the importance of fiber spacing and lamina separation, several arrangements of fibers embedded in the matrix material have been tested statically using a standard Instron Testing Machine. For this series of tests, only the metal fibers have been used in the test configurations described in Table II. The selection of the metal fibers for obtaining qualitative and quantitative data has been due to the inherent difficulties in working with glass rovings which spread during winding, appeared to have a low transverse shear failure threshold, and which could not be easily gripped by conventional testing procedures.

For the steel wires tested, surface preparation of the wires before impregnation consisted of degreasing the wire in a trichloroethylene vapor bath. Tests were performed by pulling out the fiber from the matrix at several crosshead rates corresponding to the configurations indicated in Table II. A typical test specimen was nominally .1 m long by .025 m wide by .006 m thick formed by the mold procedures discussed in Section II and references [16,18]. For the various cross head speeds available with the Instron fiber pull out from the matrix was accompanied by fiber stretching; nominally about 10 per cent of the original fiber length and an accompanying 5 per cent decrease in fiber diameter as measured using a photocomparator. It was noted that for all the fibers tested here, without benefit of special surface treatment, the pull out load level was very nearly equal to the static ultimate load of the wire itself. This would appear to indicate that at a certain loading rate, tensile failure of the fiber may preempt fiber pull out. At the cross head speeds studied here such events were not observed to occur. Some further results noted were:

- (a) increasing the crosshead speed raised the threshold force necessary to initiate fiber debonding, (b) the debonding force for complete fiber pull out remained higher for higher cross head speeds, (c) there is some influence of interfiber spacing on the load necessary for fiber pull out as evidenced by larger frictional forces remaining after full debonding has occurred (this occurs for single fibers sandwiched between laminae as opposed to multiple fibers sandwiched between laminae and may be as much as 25-30% higher) (d) varying the interlamina spacing appears to be less significant on the resultant fiber pull out.

4.3 Static and Dynamic Flat Beam Tests

Static and dynamic tests were performed on flat beam [or strip plate] specimens nominally .025 m wide by .006 m deep and .1 m long loaded in the thickness direction (perpendicular to the 0°-90° fiber directions). For the steel composites, two types of static bend tests were run, one involved specimens with the nominal dimensions indicated above, while the second involved specimens with predrilled central holes, equal in size to the impactor as used in the dynamic tests, on one side or both sides of the test specimen (see Fig. 7). The latter tests were run to simulate statically the cutting effect of the entrant penetrator and how the subsequent lamina/laminae would respond under the loading ram. These types of specimens were also used in dynamic tests in attempts to study crack initiation and growth at the reentrant corners of the cut laminae. Such static type tests were not performed on the glass epoxy specimen types because of machining problems in cutting through single glass lamina. However, dynamic tests on such specimens were conducted using fixed cutting depths.

A summary of the non-cut test specimens studied dynamically has been indicated in Table II. Results of this test program are discussed below. For the steel-epoxy beam specimens tested statically as shown in Fig. 6 the development of a generator strip was not observed. For the fiberglass specimens, however, such a development was noted. This development was particularly noted as the cross-head speed was increased. For the drilled steel specimens an adequate measure of the speed of crack propagation was not found possible. However, some recent experiments using larger notched type specimens fabricated with embedded brittle resistive wires appear to be potentially useful for such measurements.

Tests performed on the fiberglass-epoxy composites consisting of either midplane symmetric or asymmetric laminae show repeated evidence of failure on the tensile side of the strip, with delamination occurring at the interlaminar plane farthest from the midplane on the tensile side. This type of failure has also been observed in dynamic drop tests on similar types of fiber composites and reported on in reference [12]. These results suggest the conjecture that the interlaminar shear strength is significantly lower in the presence of a superimposed tension field.

Dynamic impact tests of the single and repetitive types were also conducted on both the steel-epoxy and glass-epoxy systems using the air gun assembly described in Section III, part 4 and the test fixture shown in Fig. 6. For the steel-epoxy system penetrator impact was initiated for both the predrilled and nondrilled beam specimens at various impact speeds ranging from 5.8 to 71.2 m/sec. in order to study interlaminar shear failure.

Multiple fiber specimens sandwiched between multifilament laminae were first examined in specimens with holes drilled in the front and back faces of the specimen. The machined holes were made slightly larger than the diameter of the projectile to ensure penetration contact over the machined target area. It was found that for impact velocities of 12.7 m/sec a partial delamination and generator strip formation was observed while for the steel epoxy specimens a slightly different initial failure mechanism occurred this being a conical type failure surface with radial failure lines which enlarge from the front to rear surface of the specimen. For repeated impacts at velocities between 15-25 m/sec a progressive radial failure in the form of a cone is generated while for impacts above approximately 25 m/sec an apparent symmetric localized plug type failure occurs. These results are indicative of a threshold velocity which would produce a change in the failure mode from a conical symmetric failure envelope to a localized shear plug.

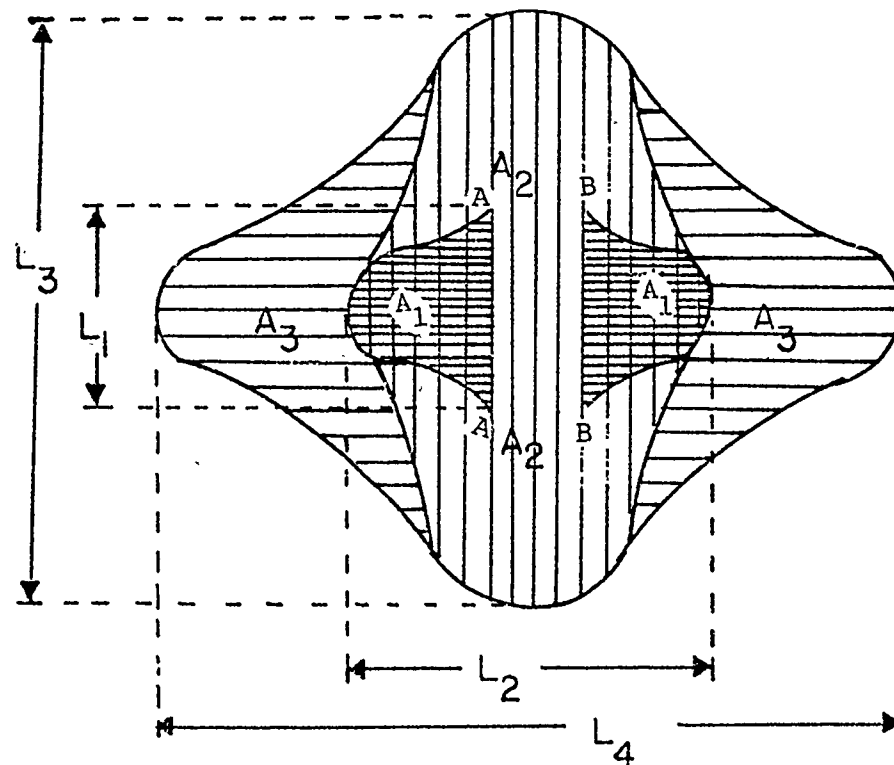
For the non-drilled composite specimens, the threshold velocity levels at which the above described phenomena occur are necessarily increased. Failures of the steel epoxy specimens were similar to those described above while for the glass epoxy specimens an intermediate fracture mechanism was observed. This mechanism consisted of unsymmetric pyramidal crack growth, with generator strip formation evident for impact velocities greater than that associated with this transition regime.

4.4 Impact Tests

Plate Impact Tests were performed on the steel-epoxy and glass-epoxy mandrel wound specimens using fixed geometry blunt ended steel impactors of nominal dimensions .008 m in diameter by .254 m long and weighing approximately 14.0 grams. The impactors were fired from the gas gun assembly shown in Figure 4 and described in section III part 4. Results obtained from previous studies of steel-epoxy plates have indicated increased penetration resistance for such material types with localized radial failure patterns, reference [4]. For the fiberglass-epoxy specimens the delamination mechanism discussed previously has been observed and appears to be a dominant mechanism in dissipating energy for kinetic energy penetrators. The results associated with such types of failure mechanisms are the principal area of concern here. It is important to note that the delamination mechanism described occurs for fiberglass-epoxy specimens fabricated by different techniques including matrix impregnation, autoclave, and vacuum bagging techniques. Also, unless otherwise indicated, the test results presented are related to fiberglass-epoxy specimens fabricated by matrix impregnation and impacted by fixed geometry impactors.

The initial tests on fiberglass-epoxy specimens under impact loading were conducted at velocities in the neighborhood of the plate penetration velocity. These results have been reported on in [4].

For 0° - 90° fiberglass-epoxy composites, delamination occurs between laminae of different orientation. The first stage of the process consists of a through-the-thickness shear failure of the first ply along the planes AA and BB as shown in Fig. 9. These planes are separated by the distance AB which is equivalent to the impactor diameter. The shear cracks generated by the impactor proceed outward terminating when the penetrator has cut all the fibers in the front strip or when the fracture surface energy available from the stress and deformation fields falls below a certain threshold level. There is some experimental evidence obtained by the investigators to support the hypothesis that a flexural wave may be the dominant mode of deformation before sequential delamination occurs. A recent study reference [20] supports a membrane hypotheses. However, the boundary conditions and geometry of the specimens used in that study cannot be compared directly to those reported on here. In any event, the generator strip formed in the first lamina creating the delaminated area A_1 pushes forward on the second lamina initiating a second generator strip and interlamina separation zone denoted by A_2 between the following laminae and so on. The delaminated areas A_1 , A_2 , etc. have been tabulated and quantitatively assessed in the following paragraphs.



18

Based upon these results tests of a series of layered plate arrangements following the listing in Table I have been conducted. The fiber plies used in each lamina of the laminate have been arranged in ascending order with an appropriate code letter at the left column of the table used to identify the plate configuration tested. The impact velocities selected for study were well below the plate penetration velocity in order to examine the sequential delamination model. For several of the plate types investigated a velocity scan was performed, testing a fixed plate type at increasing impact speed. A second series of tests examined the effect on the resultant delamination patterns of changes in the laminar stacking sequence. The quantitative measures used for reducing the data obtained were the dimensional change of the generator strip with impact velocity and plate configuration, and the total delamination area incurred. Plots of the generator strip length versus impact velocity are shown for several of the plate configurations tested in Figs. 10-11. Essentially the generator strip is observed to grow as the impact velocity is increased with approximately all curves having the same initial slope. Deviations from this norm are observed to occur when there is a thin first layer and the impact velocity is increased to a value above that necessary to initiate the process. It should be noted that the horizontal slope in Fig. 11 for the 5-4-3-2-1 configuration indicates a generator strip run out to the clamped boundary support while for the 1-2-3-4-5 configuration this represents penetration. Figure 12 shows the delaminated area plotted versus the kinetic energy of the penetrator for two of the basic ply configurations for which the delaminated area could be more easily discerned. A straight line plot through this data can be fitted and shown to be of the following form:

$$K = 3.5 + .315 A$$

where K is the kinetic energy in Joules and A is measured in cm^2 . The implication of this result is that for one fixed projectile geometry and plate type, the total delaminated area is a linear function of kinetic energy for impacts above a threshold velocity. Also, once started the delamination fracture surface energy remains constant and equal to 0.158 J/cm^2 . This corresponds to a value an order of magnitude greater than that obtained for pure epoxy as reported in reference [2] and measured from static tests. The data plotted represent that for two principal plate type configurations, specifically types i and o. The deviation from straight line behavior for the type o plate occurs due to delamination extending outward to the plate boundaries for the velocities indicated. In addition, the triangular point indicated in the diagram corresponds to results obtained on a .30 m square plate. Additional results for the mandrel wound glass-epoxy plates tested are presented in reference [19].

In addition to the experiments described above for fixed geometry impactors against matrix impregnated fiberglass-epoxy plates, a limited number of tests were conducted with different impactor masses projected against the autoclave fabricated plates of the type, b, i, o as indicated in Table 1. It has been emphasized previously that for 0° - 90° orthotropic plate specimens impacted at

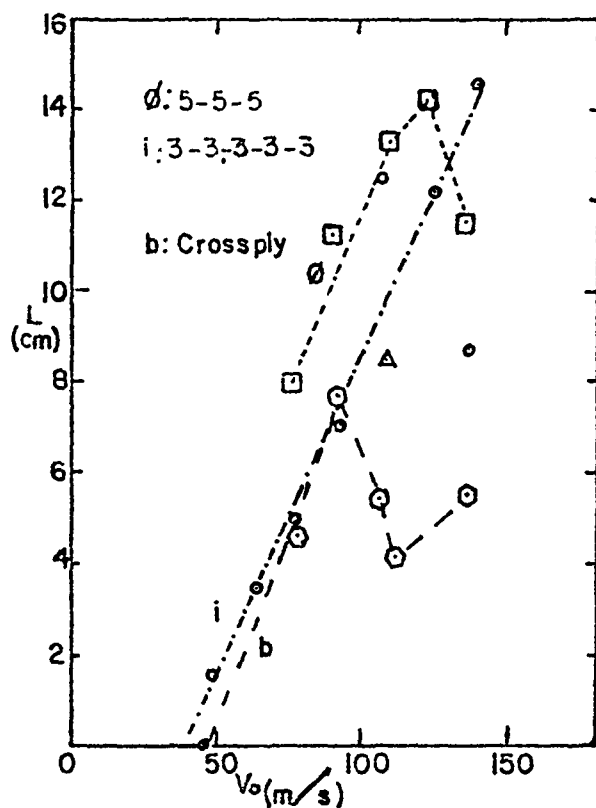


Figure 10. First generator strip length L versus impact velocity V_0 for three symmetrical layering arrangements. Point marked with triangle is for 30-cm-square 3-3-3-3-3 plate.

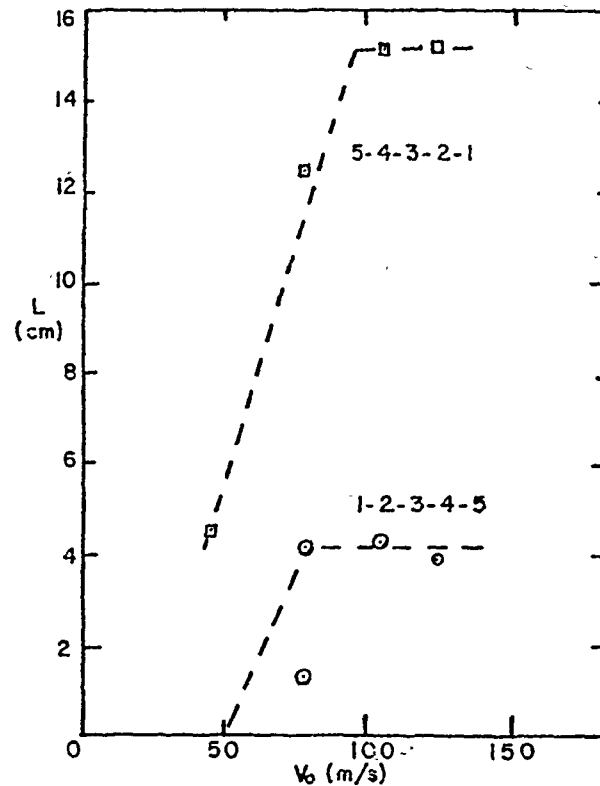


Figure 11. First generator strip length L versus impact velocity V_0 for plates with increasing and decreasing numbers of layers per lamina.

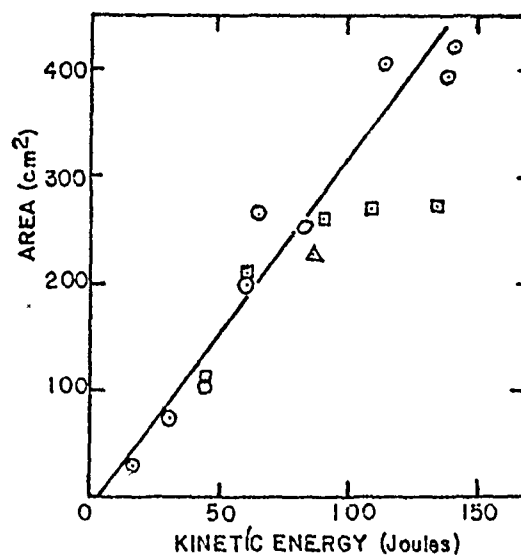


Figure 12. Total delamination area versus impactor kinetic energy for 3-3-3-3-3 plates (circle and triangle points and fitted line). Points marked with squares are 5-5-5 plates.

subperforation velocities, the same sequential delamination mechanism has been observed even though the method of specimen fabrication can be different. For the prepreg autoclave fabricated specimens the same geometric failure patterns have been observed; however, these have occurred at somewhat higher impact velocities as compared to the matrix impregnated plates. This can be attributed to some change in the volume fraction of fibers used in the prepreg specimens. For the limited number of specimens studied, particularly of the type o for quantitative data, results of the two impactor masses tested (.008 m dia x .254 and .508 m long, weighing 14.6 and 29.2 gms. respectively) suggest that the threshold delamination velocity is highly dependent upon the plate properties but that the delamination area versus kinetic energy is less so for a given projectile. Increasing the impactor mass by a factor of two did not appear to change significantly the threshold velocity for delamination; however, the slope of the kinetic energy versus delamination area appeared to be increased by about 50%. Quantitatively, for the prepreg plates of type o the average threshold kinetic energy for delamination for the one inch impactor was 9 Joules versus 3.5 Joules for the matrix impregnated plates. The corresponding number for the two inch impactors is approximately 29 Joules. These results are considered very important; but an insufficient number of tests have been conducted to warrant any definitive quantitative statements.

4.5 Blast Loading

In addition to the blunt nose penetrator impact tests run on the fiberglass-epoxy plates, a series of blast load tests were run on glass-epoxy plates as fabricated from the basic constituent materials, from prepreg Scotchply 1002 tape, and from woven fiberglass cloth. The loading on these plates has been described in section III part 5. A visual inspection of these plates using back lighting has disclosed the following type of delamination mechanism.

At loads less than that required to fail the plates along the boundaries, delamination begins at the edges and progresses toward the center of the plate. The amount of delamination occurring appears to be closely related to the blast pressure and/or plate deflection. Delamination on the first interlaminar plane occurs on the edges normal to the fiber direction of the first lamina. The next delamination occurs on the next interlaminar plane extending outward from the other two edges. This process is repeated in an alternating sequence through the thickness of the specimen and through all the interlaminar planes with an observed decreasing delaminated area formed. A schematic of this delamination pattern is shown in Fig. 13 with the total number of contributing planes to the delamination process readily apparent particularly for low numbers of interlaminar planes. The large sized plate configurations tested (.30 m square) were of the type indicated in

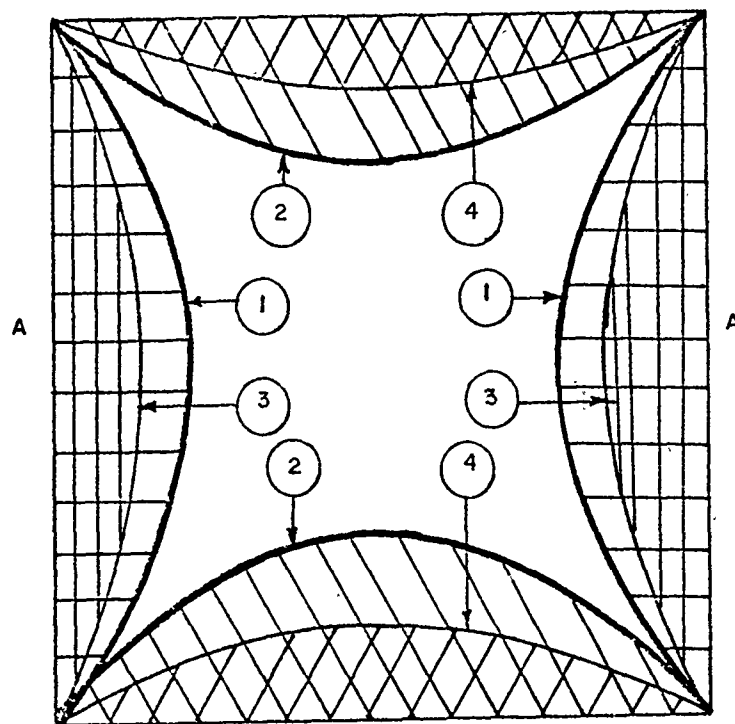


Figure 13. Schematic of delamination mechanism for blast loaded plates. Representative of a five lamina plate. Circled numbers refer to delamination sequence increasing from front to back. Edges marked A are perpendicular to fibers in first lamina.

Table I. The relation between the delaminated area and the peak blast pressure generally follows a linear relation as shown in Figure 14 for the two types of cross plied plates analyzed. From previous results, it has been shown using a shadow Moire technique [22] that a plate of type i deflected as much as 3.81 cm at the center under a blast load and rebounded to a final permanent set of .64 cm at the center. Considering the rebounded work as elastic, the unrecovered work can be considered transferred to the plate. A rough analytical estimate of this unrecovered work can be obtained by integration of the permanent deflection times the blast pressure acting over the plate area. Both the time required for plate deflection and rebound have been noted to be of the same order of magnitude as the blast duration time and therefore only half the peak pressure has been used in the subsequent calculations. A plot of this unrecovered work versus delamination area is shown in Fig. 15. The curve appears to be linear over the range shown with a constant slope of $0.826 \text{ Joules/cm}^2$

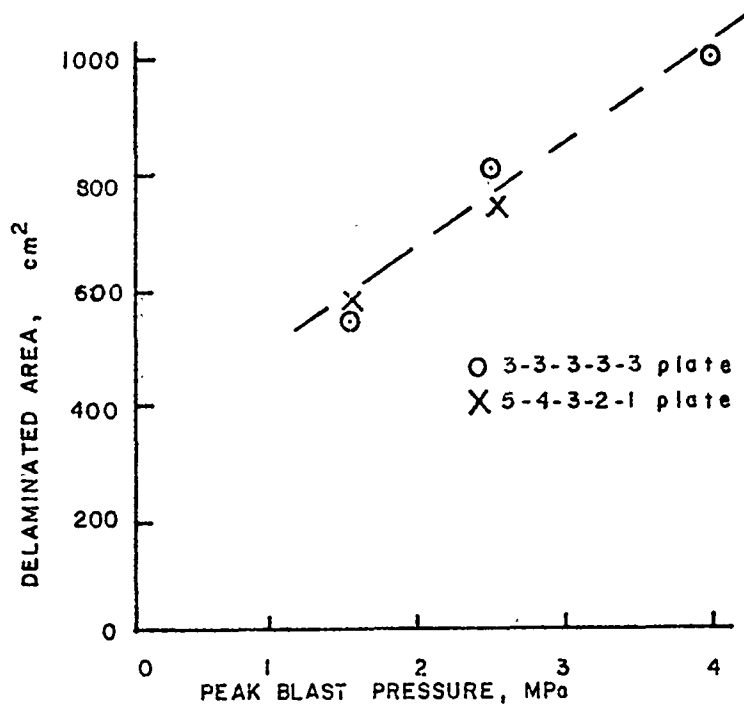


Figure 14. Delaminated Area Versus Peak Blast Pressure

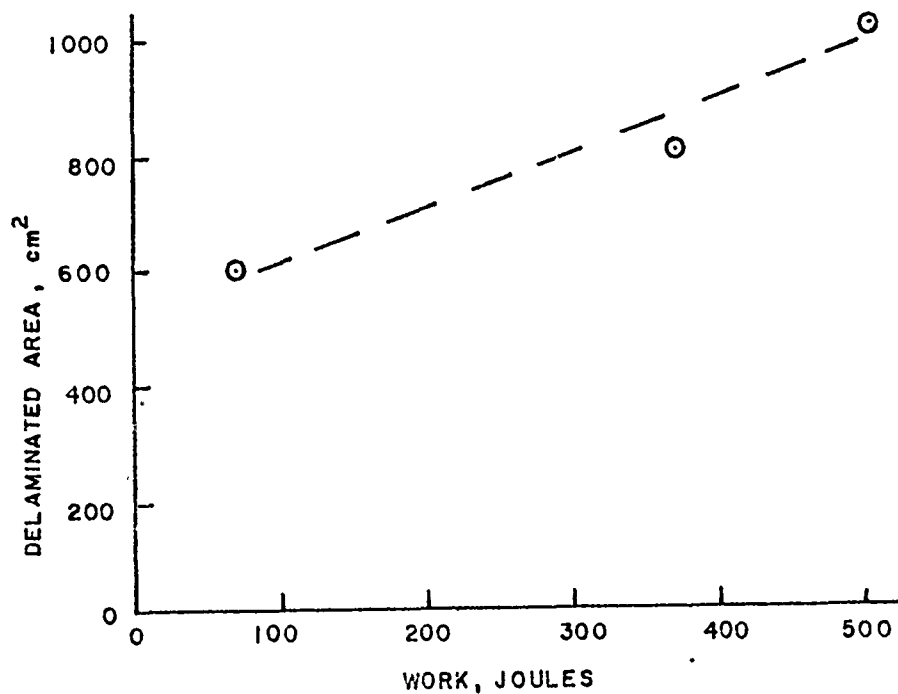


Figure 15. Delaminated Area of 3-3-3-3-3 Plate Versus Unrecovered Work

corresponding to a fracture surface energy of $0.431 \text{ Joules/cm}^2$. This value of the fracture surface energy is of the same order of magnitude as that obtained in the previously discussed plate impact tests. The results obtained for these tests were found to occur for both the large sized plates fabricated using the matrix impregnation and for the Scotchply prepreg types.

Tests were also performed on fiberglass cloth weave plates of various sizes and thicknesses. Blast loading of the nominally .25 m square fiberglass weave plates displayed once again a delamination mechanism which extended from the plate edges toward the plate centers. Because of the ease of fabrication of fiberglass cloth, plates of two widths (25 cm and 46 cm) and two thicknesses (.64 cm and .32 cm) were tested. The .32 cm thickness plates for both widths showed very little delamination but instead displayed a uniform craze type pattern which might be expected for a highly stressed membrane type of composite plate. The thicker .64 cm plates of 46 cm width show a delamination pattern very similar to that of the plates previously described.

5. ANALYSIS

5.1 Plane Stress Plate Bending

5.1.1 Introduction

The bending response of flat plates to both static and dynamic loads has been treated by many authors, and it would be ambitious to attempt a listing of all pertinent publications. However, for general information the reader is referred to the classical elastic plate text by Timoshenko [23], the theory of anisotropic plates by Ambartsumyan [24], and the application of classical plate theory to laminated plates by Ashton and Whitney [25].

It is realized that the delamination process as described earlier using the generator strip mechanism may not be analyzed exactly using classical plate theory, but some insight into the stress distribution may be gained from such an analysis. Classical plate theory may be defined in terms of the assumptions made for the strain-displacement relations used in the analysis. The strain-displacement assumptions as used in classical plate theory are: (1) strains are small compared to unity, (2) the thickness of the plate is small compared to other dimensions and (3) normals of the undeformed surface remain normal to the deformed surface and are not elongated, thus neglecting transverse shear and normal strains in the plate deflection analysis. Neglecting transverse shear strains would imply negligible transverse shear stresses, and indeed they are small in comparison to the bending stresses. Since they are, however, important in connection with delamination, they may be estimated by considering the inplane equations of motion. For symmetric loading normal to a plate the inplane shear and inertial forces are negligible and variations of transverse shear stresses in the thickness direction may be determined in the following manner.

The equations of motion for the inplane plate coordinates may be approximated in the undeformed x, y coordinate system and expressed as

$$\begin{aligned}\frac{\partial \sigma_{xx}}{\partial x} + \frac{\partial \tau_{xy}}{\partial y} + \frac{\partial \tau_{xz}}{\partial z} &= \rho \ddot{x} \\ \frac{\partial \tau_{xy}}{\partial x} + \frac{\partial \sigma_{yy}}{\partial y} + \frac{\partial \tau_{yz}}{\partial z} &= \rho \ddot{y}\end{aligned}\tag{1}$$

Imposing the previous stated assumption that the inplane shear stress τ_{xy} and the inplane inertia forces $\rho \ddot{x}$, $\rho \ddot{y}$ are negligible, reduces equations (1) to

$$\begin{aligned}\frac{\partial \sigma_{xx}}{\partial x} &= - \frac{\partial \tau_{xy}}{\partial z} \\ \frac{\partial \sigma_{yy}}{\partial y} &= - \frac{\partial \tau_{yz}}{\partial z}\end{aligned}\tag{2}$$

For finite variations in position Δz the shear stress variations may be approximated as

$$\begin{aligned}(\tau_{xz})_2 &= (\tau_{xz})_1 + \frac{\partial \tau_{xz}}{\partial z} (\Delta z)_{1-2} \\(\tau_{yz})_2 &= (\tau_{yz})_1 + \frac{\partial \tau_{yz}}{\partial z} (\Delta z)_{1-2}\end{aligned}\tag{3}$$

By using equations (2) in equations (3) and a zero shear stress at a free surface for shear stresses $(\tau_{xz})_1$ and $(\tau_{yz})_1$ the shear stresses at some position z between the top surface and the plate midplane are obtained as

$$\begin{aligned}\tau_{xy} &= \frac{\partial \sigma_{xx}}{\partial x} \Delta z \\ \tau_{yz} &= \frac{\partial \sigma_{yy}}{\partial y} \Delta z,\end{aligned}\tag{4}$$

where Δz is measured downward from the upper surface of the plate.

In the present study, analysis for selected fiberglass-epoxy plates has been accomplished using an elastic orthotropic multi-layered panel option of a computer code entitled DEPROP, an acronym for a digital computer program for predicting the Dynamic Elastic-Plastic Response Of Panels to Blast Loadings [26]. The study considered both blast type and concentrated impact loadings for comparison with test data.

Uniform loading on a blast loaded plate can be treated rather simply by the code since the code has incorporated within it a loading option designed specifically to handle such loads. For concentrated central impacts, however, a modified analysis is required in that some simple assumptions must be made so that the impact can be considered as some large pressure load applied over a small area. The length of time t_c that the projectile was in contact with the plate was determined experimentally and used with the momentum of the projectile, to calculate a specific impulse \bar{I} . This impulse may be expressed as

$$\bar{I} = \frac{mv}{A}\tag{5}$$

where m , v , and A are respectively, the mass, impact velocity and cross sectional area of the cylindrical projectile.

For the calculations this impulse was assumed to be applied as a pyramidal shaped pressure distribution over a square area at the center of the plate with side length equal to the projectile

diameter. The maximum pressure was assumed instantaneously applied and then decreasing linearly with time to give a triangular pressure-time function.

5.1.2 Impact Analysis

Simulated impact analyses were made on various plate types for several impact velocities. Emphasis was, however, placed on the three and five lamina plates for velocities between 46 m/sec. (150 fps) and 152 m/sec. (500 fps). Preliminary analysis showed similar results for all plate configurations. Therefore, only two plate configurations were analyzed rather extensively. Also, because computer costs became a factor, a selective analysis of those plate types which had been most extensively tested was given first priority.

It is important to note that all the analyses made on the composite plates are elastic dynamic solutions. Large deflection theory was used but was completely elastic. The analysis would be reasonably good up to plate delamination. However, experimental evidence indicates that plates remain fairly elastic even after large delamination damage has occurred.

Typical results for σ_{xx} versus x are given in Figures 16a and 16b for the three-lamina^{xx} plate for an impact velocity of 107 m/sec. A sketch given at bottom of Table III shows the line BC represented by the abscissa in Figures 16a and 16b. The slopes of these curves yield $\partial\sigma_{xx}/\partial x$ and when used in equations (4) provide an approximation for the interlaminar shear stress τ_{xz} . For example, for the three lamina plate, by calculating the average value of $\partial\sigma_{xx}/\partial x$ between the top and bottom of the top lamina, an approximate shear stress τ_{xz} was calculated, which is tabulated as a function of time in Table III for two different impact velocities. The stresses of Table III were calculated for a point 1.27 cm. from the center of the plate as shown at the bottom of Table III. This stress τ_{xz} is only one component of the shear stress at this point. The shear stress τ_{yz} acts at 90° to this stress and is comparable in magnitude, giving a resultant shear stress approximately 1.4 times that of Table III. The interlaminar shear strength for the plates analyzed is not known but estimated to be approximately 17.25 MPa (2500 psi) or about 60% of 28.3 MPa (4100 psi) the reported interlaminar shear strength of the commercial Scotchply epoxy-glass laminates. This estimate is based on a 4-6% void content present in the plates tested which according to [27] may give rise to a 40% decrease in shear strength.

The stresses shown in Table III are those of the interlaminar shear stress for the interlaminar plane between the top and middle lamina of a three lamina plate. The variation of τ_{xz} with z through the plate thickness for point D in the sketch of Table III, is shown in Figures 17a,b. The results show that the shear stress

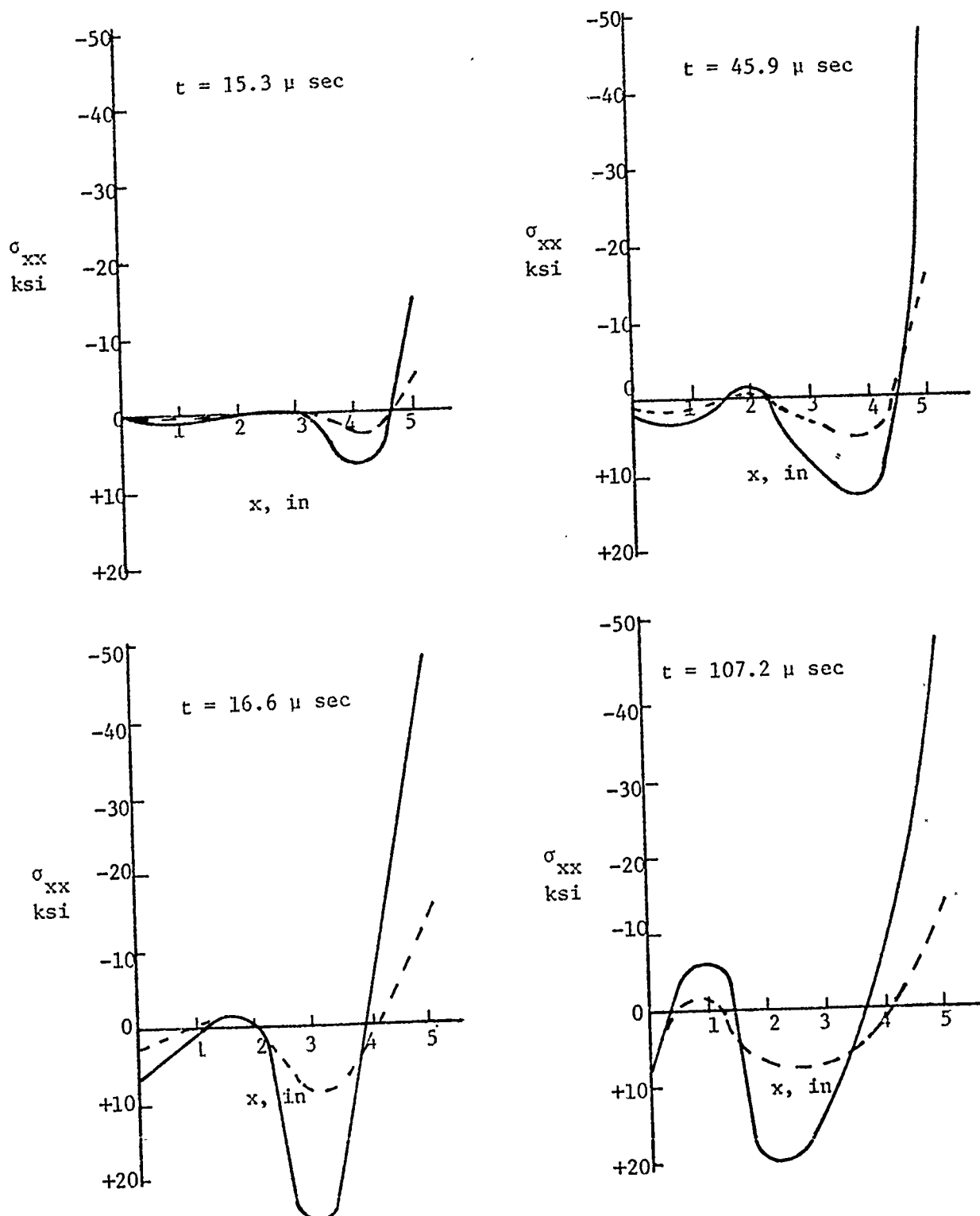


Figure 16 a σ_{xx} versus x coordinate across center of three lamina plate with 150 FPS central impact. See Table III for point of plate analyzed. Zero time at impact. Solid curve represent stress on top of upper lamina and dotted curves represent stress on bottom of upper lamina.

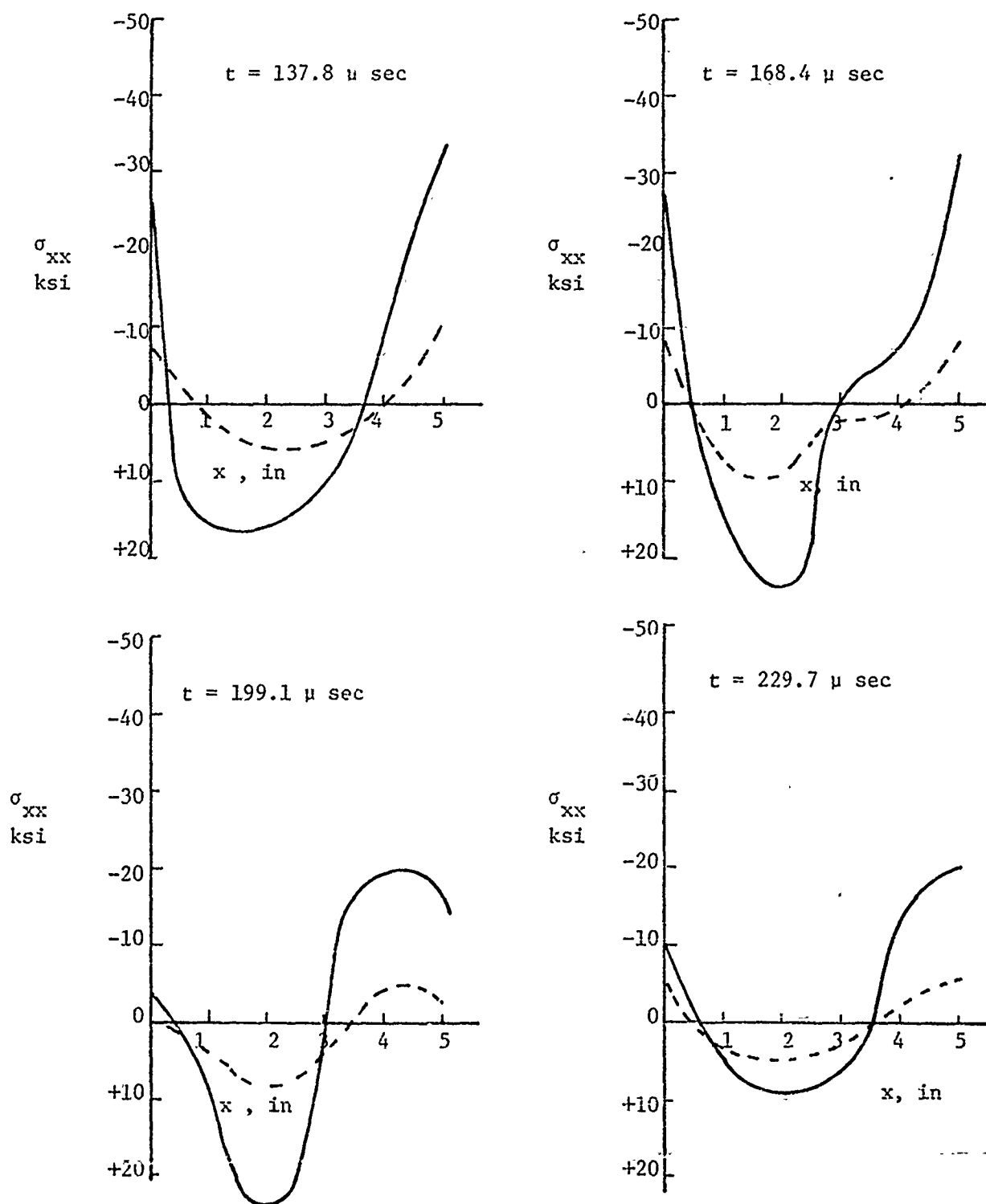
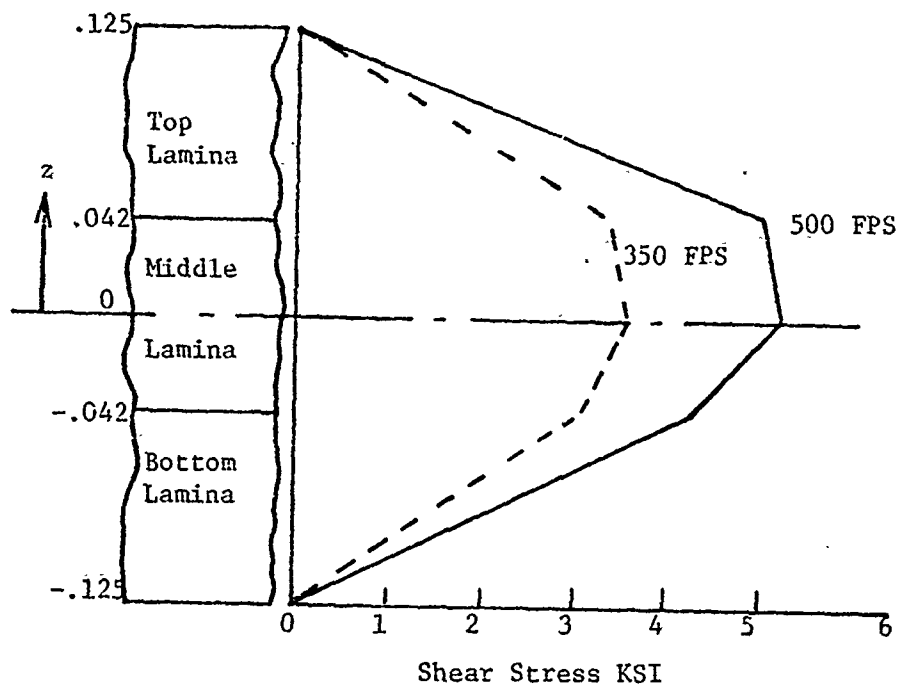
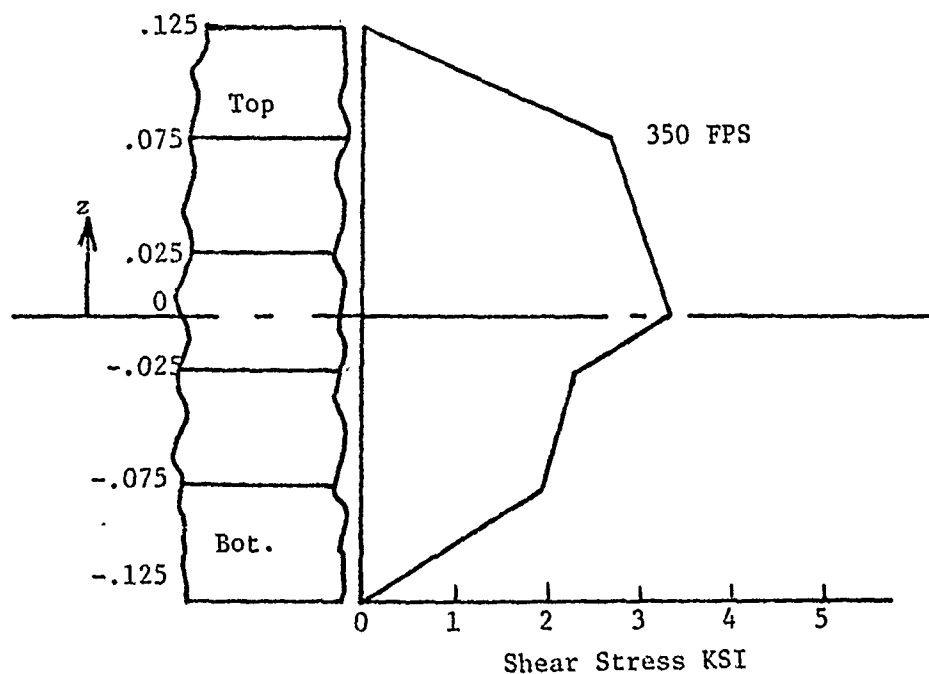


Figure 16 b Continuation of Figure 16a of σ_{xx} vs x coordinate. See Table III for position of plate analyzed. Zero time at impact.



(a) Three Laminae



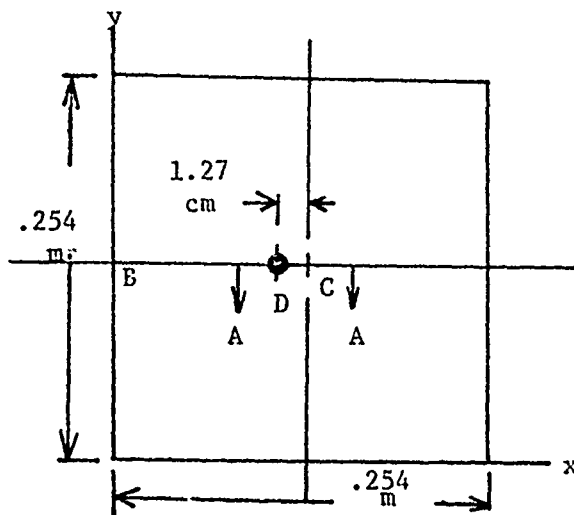
(b) Five Laminae

Figure 17. Shear stress τ_{xz} distribution through plate thickness for three and five lamina plates with impact loads.

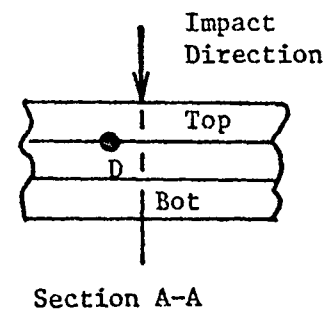
TABLE III

Interlaminar or Transverse Shear Stress τ_{xz} for a Three Lamina Plate at 1.27 cm. from Plate Center.

Time after impact usec.	Shear Stress τ_{xz} , MPa (Psi) for given impact velocities.	
	107 m/sec.	153 m/sec.
15.3	8.28 (1200)	11.87 (1720)
30.6	17.53 (2540)	25.32 (3670)
45.9	23.25 (3370)	33.60 (4870)
61.3	21.39 (3100)	31.74 (4600)
76.6	16.84 (2440)	24.01 (3480)
91.9	16.91 (2450)	23.81 (3450)
107.2	16.63 (2410)	23.05 (3340)
122.5	11.11 (1610)	14.70 (2130)
137.8	8.83 (1280)	11.45 (1660)
153.1	7.73 (1120)	10.14 (1470)



Point analyzed in above Table III



risers very rapidly through the first one or two laminae near the top or bottom because of high values of σ_{xx} and $\partial\sigma_{xx}/\partial x$ on the top and bottom of the plate. The shear stress then increases less rapidly to a maximum at the midplane. This was also observed for a 15 lamina plate impacted at 107 m/sec. A general observation in these cases is that the interlaminar shear stresses for all interlaminar planes are of approximately the same order of magnitude, suggesting that the probability of delamination occurring in any of the interlaminar planes is about the same. This analysis does not

predict which interlaminar plane may fail first but does show that the shear stresses occurring may be of sufficient magnitude to produce delamination even for low impact velocities.

5.1.3 Blast Analysis

Analyses using the DEPROP code were also performed on several plate configurations for the blast loadings tested experimentally. Some typical results are given in Figures 18a,b,19 for the line BC and point D analyzed as shown in Figure 20. Note that the negative stress for these curves is plotted upward in keeping with the same sign convention used in Figures 16a, b.

For the impact case the higher stress occurs first at the center of the plate and engulfs the plate from the center outward as evidenced by the higher stresses at the $x=5$ positions for the curves shown in Figures 16a, b. However, for the blast loading the reverse occurs in that the higher stress occurs first at the fixed edges or $x=0$ for the curves in Figures 18a,b. This result has been observed experimentally when plate deflections are monitored or for post impact inspected back lighted plates. For these cases, the delamination progresses from the center outward for central impact loads and from the plate edges inward for blast loads.

Comparisons between the analysis for the two types of loads must be made with extreme care but in general the failure mechanisms appear to be similar, and some similarities are in evidence in the analyses. Even though the two types of external loading produce opposite algebraic stress resultants where the shear stress is largest that is, biaxial compression on the top and at the center of the plate for impact loads and biaxial tension on the top and at sides of the plate for blast loads, the sign of the slope of the σ_{xx} versus x curve is the same for both. This leads to the same sign of shear stress for both cases. Additional general observations are;

1. For impact loaded plates the higher the impact velocity the more delaminated area is found in the plate. The analysis for a given point gives higher shear stress for the higher impact velocity.
2. For blast loaded plates the higher the blast load the more delaminated area is found in the plate. The analysis for a given point gives a higher shear stress for the higher blast loads.
3. More delaminated area is found in a plate with 375 psi blast load than for a 150 fps impact load. The comparison of the two analyses for these cases verifies this in the sense that it predicts high shear stresses over a greater area of the blast loaded plate.

The analysis presented here for the loading cases considered is indeed in no way comprehensive. However, some trends are

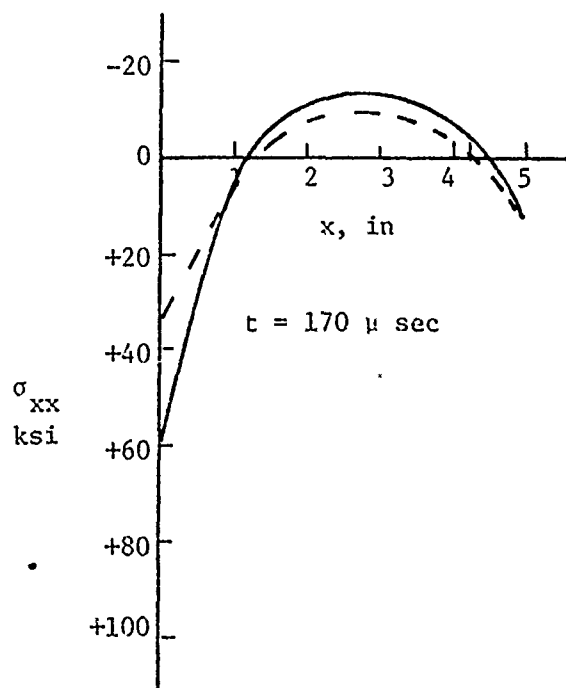
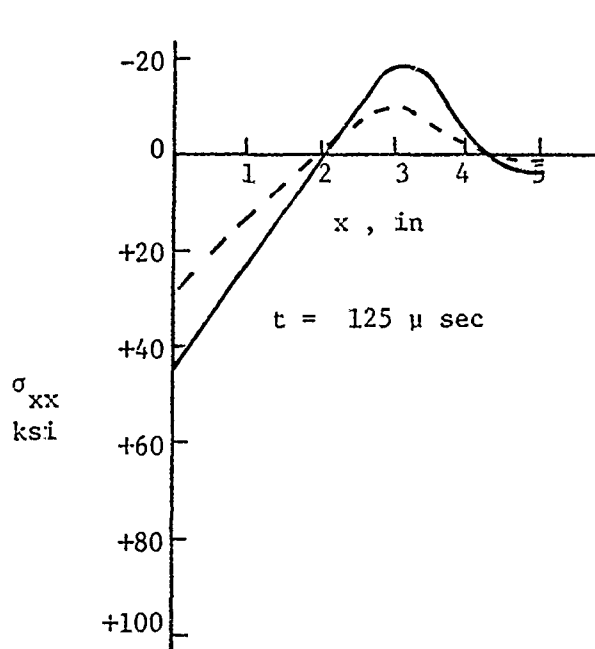
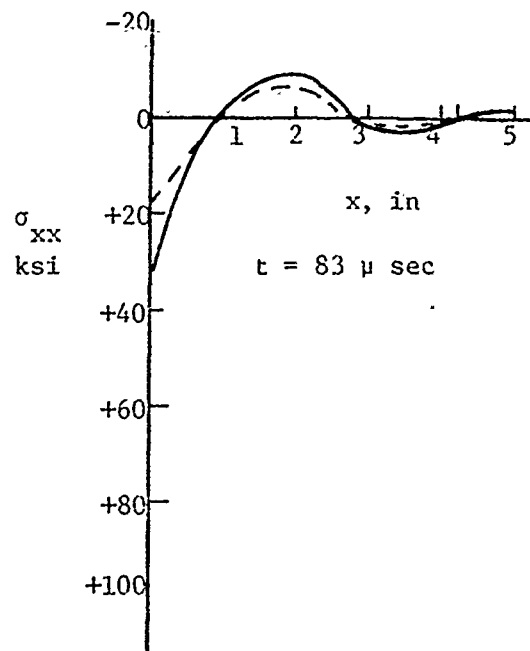
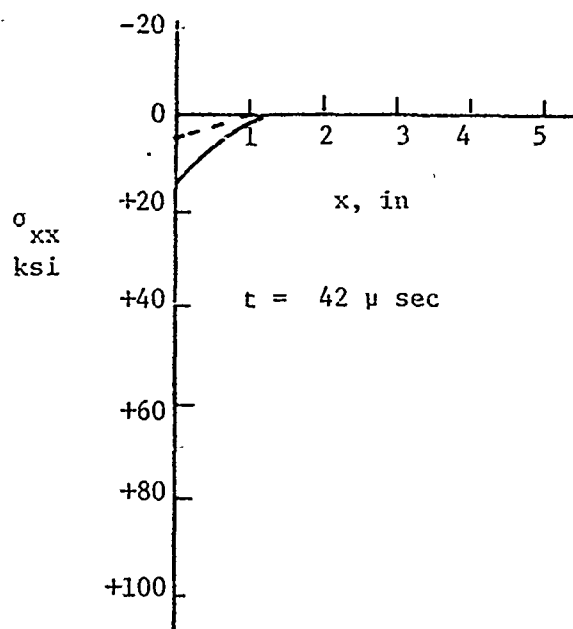


Figure 18 a σ_{xx} versus x coordinate across center of five lamina plate for 375 psi blast load. See Figure 20 for positions of plate analyzed. zero time at beginning of blast. Solid curve represents stress on top of upper lamina and dotted curve represents stress on bottom of upper lamina.

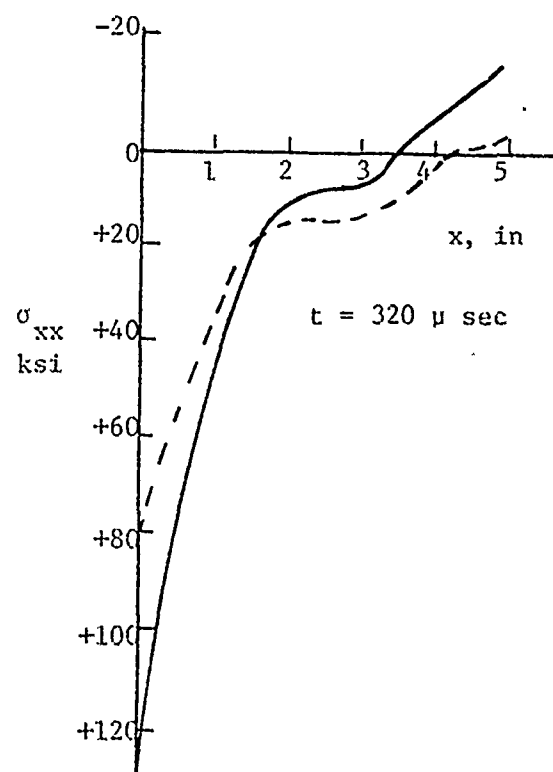
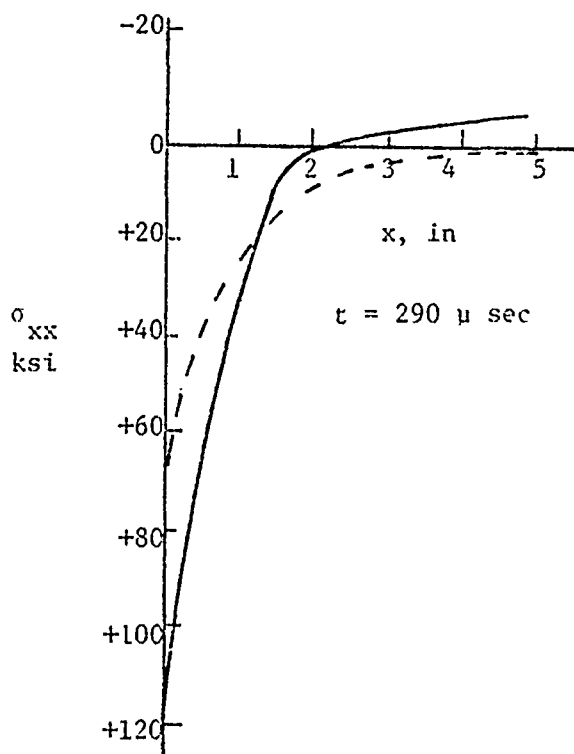
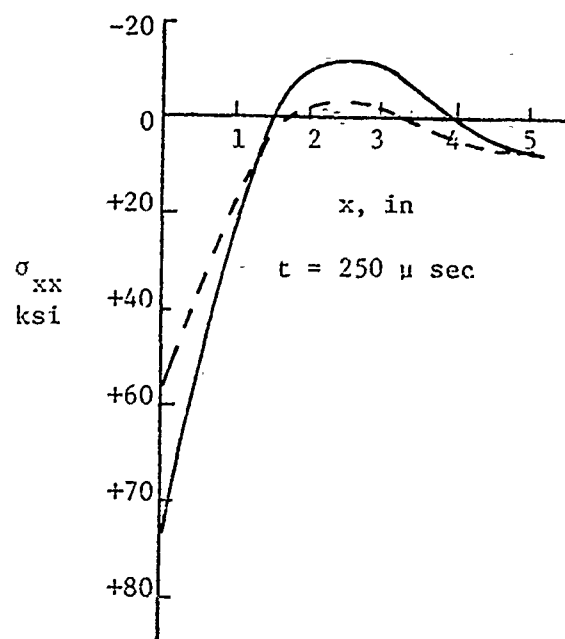
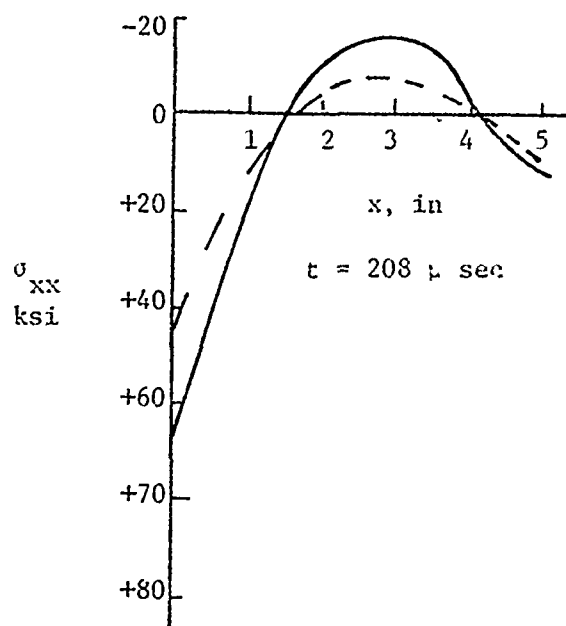


Figure 18 b Continued

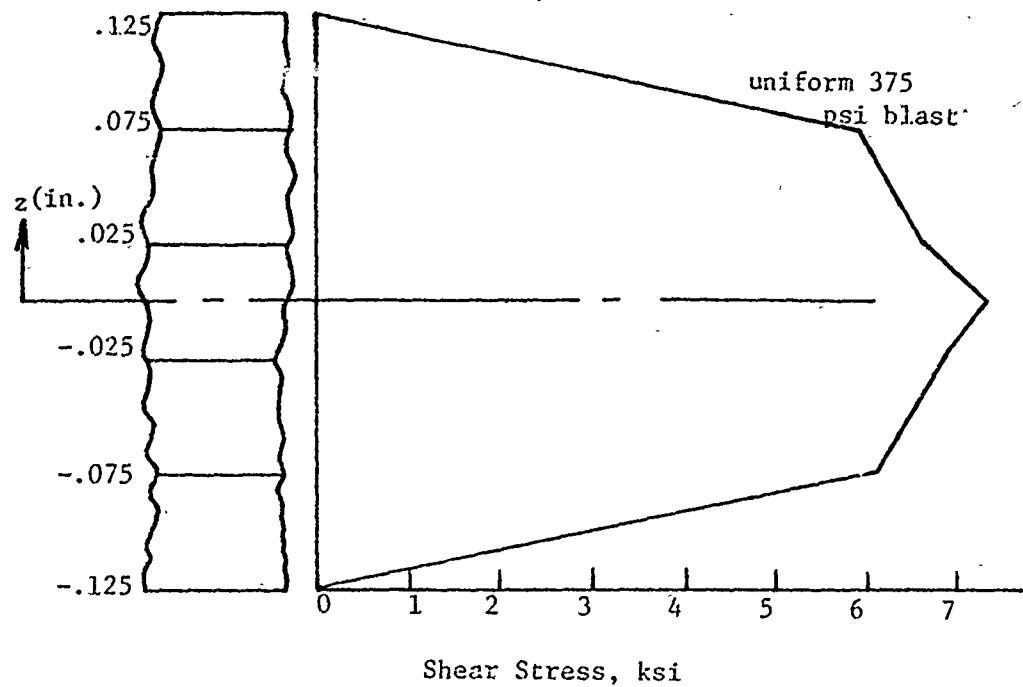
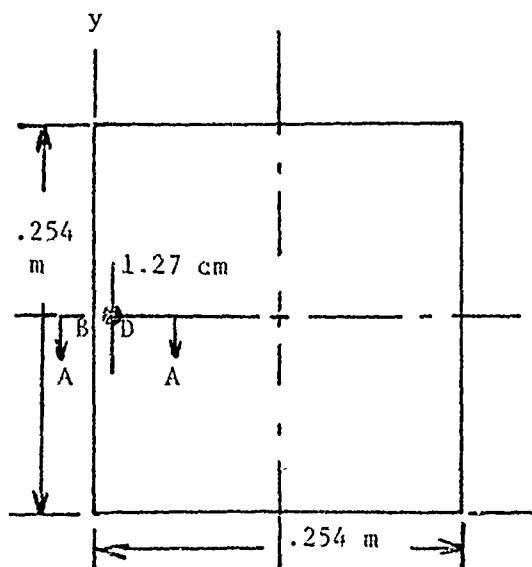


Figure 19 Shear stress τ_{xx} through thickness for five lamina plate with blast load.



● Point analyzed in Figures 18-19

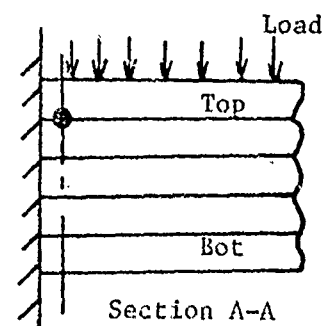


Figure 20 Position of points analyzed in Figures 23-25.

evidenced and additional work into modifying the DEPROP code to calculate the shear stresses directly might be in order. Essentially the main conclusion reached here is that a plane stress classical plate theory can be a useful first order tool for predicting interlaminar shear stresses in dynamically loaded composite plates.

5.2 Cylindrical Bending of 0°-90° Laminated Plates with Orthotropic Laminae

5.2.1 Introduction

In the dynamic elastic analyses of Sec. 5.1 the maximum shear stress appeared to be at the midplane. The flexural shear stress profile was fairly flat except near the top and bottom surfaces, so that the predicted interlaminar shear stresses were of the same order of magnitude in all interlaminar planes for the cases analyzed (3, 5, or 15 laminae).

In the dynamic experimental investigations the first interlaminar plane to delaminate appeared always to be the interlaminar plane nearest the loaded surface rather than one nearest the midplane. This might be attributed to the generator-strip mechanism in the case of the centrally impacted plates, but not in the blast loaded plates, for which the delamination began at the clamped boundary on the interlaminar plane nearest the surface, where the bending stress was tensile. For static loading of flat-strip beams in three-point bending, the first delamination occurred on the opposite side from the central load, i.e. at the interlaminar plane nearest the surface on the tension side.

It was suggested that the shear failures on the tension side might possibly be explained by the unequal elastic moduli in tension and compression, which could cause the maximum flexural shear stress to be at some distance from the midplane. A few calculations for static cylindrical bending of uniformly loaded glass-epoxy plates of typical material properties have shown, however, that the maximum flexural shear stress still occurs near the midplane. The greatest distance found in these calculations was about $0.1h$ for plate thickness h in a 5-lamina 3-3-3-3-3 stacking sequence plate, which is not enough to explain the initial failure by delamination at a distance of $0.3h$ from the midplane ($0.2h$ from the tension side). No such calculations have been made for the dynamic loadings. The calculation method is briefly outlined in the following section.

5.2.2 Static Cylindrical Bending Analysis for 0°-90° Laminated Plates with Orthotropic Laminae

The usual Kirchhoff bending assumptions of classical plate theory lead to the following equations, as, for example in [25], for the midsurface deflection $w(x)$ in the z -direction and midplane

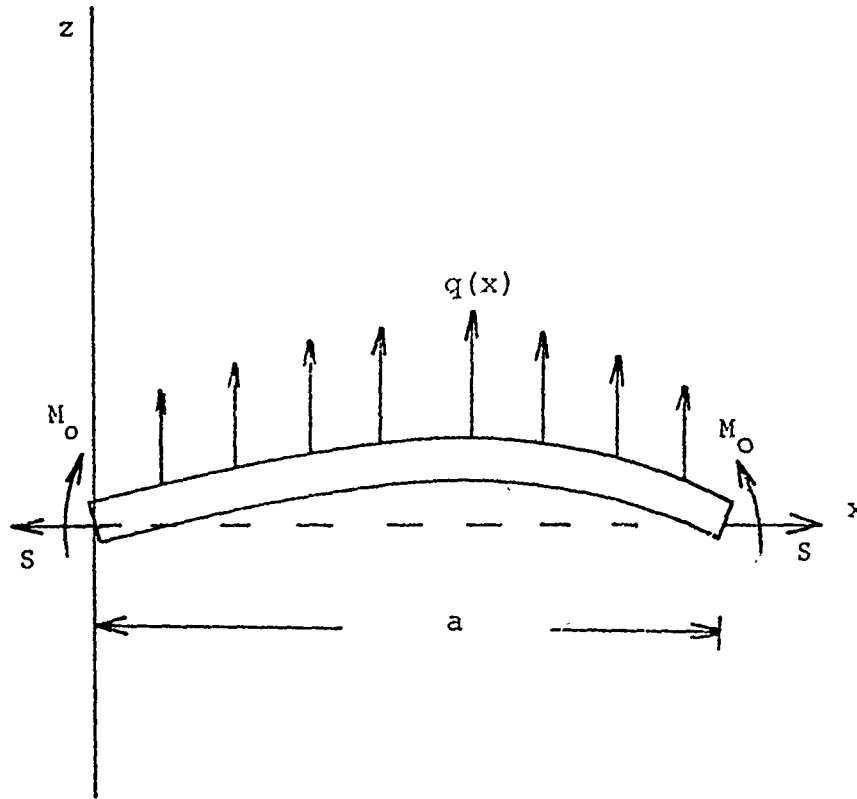


Fig. 21. Cylindrical Bending Configuration

strain $\varepsilon^o(x)$ in the x-direction for cylindrical bending of the plate shown in Figure 21.

$$A_{11} \frac{d\varepsilon^o}{dx} - B_{11} \frac{d^3 w}{dx^3} = 0 \quad (6)$$

$$D_{11} \frac{d^4 w}{dx^4} - B_{11} \frac{d^2 \varepsilon^o}{dx^2} - S \frac{d^2 w}{dx^2} = q \quad (7)$$

where

$$A_{11} = \int_{-h/2}^{h/2} \bar{Q}_{11} dz \quad B_{11} = \int_{-h/2}^{h/2} \bar{Q}_{11} z dz \quad (8)$$

$$D_{11} = \int_{-h/2}^{h/2} \bar{Q}_{11} z^2 dz$$

$$\bar{Q}_{11} = \frac{E_1}{1 - \nu_{12}\nu_{21}} \quad \text{in laminae with fibers in the x-direction} \quad (9)$$

$$\bar{Q}_{11} = \frac{E_2}{1 - \nu_{12}\nu_{21}} \quad \text{in laminae with fibers in the y-direction}$$

The boundary conditions are

$$w(0) = w(a) = 0$$

(10)

$$\epsilon^o(0) = \epsilon^o(a) = \frac{1}{D} [D_{11}S + B_{11}M_o]$$

$$\frac{d^2w}{dx^2} = \frac{1}{D} [M_o + B_{11}S] \quad \text{at } x=0 \text{ and } x=a$$

where $D = A_{11}D_{11} - B_{11}^2$.

The Kirchoff bending assumptions imply bending strain

$$\epsilon_{xx} = \epsilon^o - z \frac{d^2w}{dx^2} \quad (11)$$

linear in z , from which the lamina bending stress σ_{xx} in lamina k can be calculated by

$$\sigma_{xx} = \bar{Q}_{11}^{(k)} \epsilon_{xx} \quad (12)$$

Ashton and Whitney [25] gave polynomial solutions for simply supported plates [$M_o = 0$] and for clamped plates, in both cases unrestrained against inplane motion at the boundary so that $S=0$. Other cases can be included by suitable modifications of the results given in [23] for isotropic plates.

For static loading, the membrane stress is equal to S , independent of x , and the midplane strain can be shown to be

$$\epsilon^o = (S/A_{11}) + (B_{11}/A_{11})w''(x) \quad (13)$$

where $w''(x)$ denotes d^2w/dx^2 . Substituting this into (11) gives

$$\epsilon_{xx} = (S/A_{11}) + [(B_{11}/A_{11}) - z]w''(x) \quad (14)$$

Thus the neutral surface where $\epsilon_{xx} = 0$ occurs at z^* given by

$$z^* = (B_{11}/A_{11}) - [S/(A_{11}w''(x))]. \quad (15)$$

For the unrestrained case, $S=0$ and

$$z^* = B_{11}/A_{11} \quad (16)$$

As in Sec. 5.1, we can calculate the flexural shear stress τ_{xz} by integrating the differential equation of equilibrium.

$$\partial \tau_{xz} / \partial z = -\partial \sigma_{xx} / \partial x \quad (17)$$

and using the condition that $\tau_{xz} = 0$ at $z = h/2$. Equations (12) and (14) give

$$\partial \sigma_{xx} / \partial x = \bar{Q}_{11}^{(k)} w'''(x) [(B_{11}/A_{11}) - z] \quad (18)$$

Thus, by Eq. (17)

$$\partial \tau_{xz} / \partial z = \bar{Q}_{11}^k w'''(x) [z - (B_{11}/A_{11})] \quad (19)$$

If the maximum value of τ_{xz} occurs at $z=z_1$ within a lamina where $\partial \tau_{xz} / \partial z$ is defined, then $\partial \tau_{xz} / \partial z = 0$ there, and

$$z_1 = B_{11}/A_{11}. \quad (20)$$

Equation (20) gives the location of the maximum τ_{xz} even if the derivative does not exist, as at an interlaminar plane, since the derivative changes sign there.

Although the distance z_1 to the calculated position of maximum shear stress according to Eq. (20) does not depend explicitly upon the membrane stress S , it is implicitly contained in B_{11} , since the value of B_{11} will depend on the location of the neutral surface if the tension and compression moduli are not equal, and equation (15) shows that the location of the neutral surface depends upon S .

5.2.3 Examples of Estimates for Glass-Epoxy Plates

The maximum shear stress location for a plate with three laminae, each of thickness $h/3$ was calculated under the assumption that the neutral plane was within the middle lamina and that the difference between the tension and compression moduli could be neglected in the middle lamina, whose fibers were transverse to the bending direction. The result was

$$z_1 = B_{11}/A_{11} = \frac{h}{3} \frac{E_1^t - E_1^c}{E_1^c + E_2 + E_1^t} \quad (21)$$

for the loading of Fig. 21 where the tension side is the positive z side of the plate. Here E_1^t and E_1^c are the tension and compression moduli in the fiber directions [x-directions for the two outer laminae] and $E_2^t = E_2^c = E_2$ is the transverse modulus. It was also assumed that the Poisson's ratios were the same in tension and compression.

For Scotchply, 3M XP251S, Jones [28] gives

$$E_1^t = 8 \times 10^6 \text{ psi}, \quad E_1^c = 7.5 \times 10^6 \text{ psi} = 0.9375 E_1^t$$

and

$$E_2 = 2.7 \times 10^6 \text{ psi}. \quad (22)$$

With these values the maximum shear stress for the 3-lamina plate occurs at

$$z_1 = 0.03 h \quad (23)$$

A similar calculation for the lower volume fraction E-glass epoxy

used in most of the experimental studies of the present program, with

$$E_1^t = 3 \times 10^6 \text{ psi and } E_2 = 0.233 E_1^t \quad (24)$$

and assuming $E_1^c = 0.9375 E_1^t$

as in the Scotchply case, since the compression modulus was not known, gave

$$z_1 = 0.01h \quad (25)$$

for the three-lamina plate.

For the plate with five 0° - 90° orthotropic laminae, each of thickness $h/5$ the first estimate was made by neglecting the difference between tension and compression moduli in the middle 0° lamina, where the bending stress is small anyway, as well as in the two transverse laminae. This gives

$$z_1 = 0.4h \frac{E_1^t - E_1^c}{E_1^c + 2E_2 + 2E_1^t} \quad (26)$$

The properties listed previously then give

$$z_1 = 0.095h \text{ for the Scotchply 3M XP251S} \quad (27)$$

$$z_1 = 0.008h \text{ for the E-glass} \quad (28)$$

The Scotchply five-lamina plate was re-estimated by assuming the middle lamina entirely in compression, giving

$$z_1 = 0.4h \frac{E_1^t - E_1^c}{2E_1^c + 2E_2 + E_1^t} \quad (29)$$

or

$$z_1 = 0.12h \quad (30)$$

as compared to $z=0.3h$ at the interlaminar plane nearest the surface on the tension side.

The unequal moduli may make some responses different, as Jones [29] has pointed out, but do not seem to explain the delamination on the tension side. An explanation is more likely to be found in some combined-stress failure criterion that predicts a lower shear strength in the presence of a superimposed tension field than in the presence of a compression field.

6. CONCLUDING REMARKS

The following comments summarize briefly the results obtained for central impact and for blast loading on 0°-90° layup fiber-glass-epoxy composite plates.

1. A sequential delamination failure mechanism has been shown to exist for filamentary composite fiberglass-epoxy plates of various fiber weight percents, fabricated by various standard methods.
2. For the centrally impacted plates the development of the delamination mechanism was associated with a generator strip mechanism. When the first lamina had enough fiber layers to prevent immediate perforation, a strip formed by through-the-thickness cracks in the first lamina loaded transversely the second lamina. This generator strip length increased (for a given impactor speed and mass) when the number of fiber layers in the first lamina was increased.
3. For fixed plate geometry and lamina orientation and a given central impactor geometry and mass, the total delaminated area appears to be a linear function of the impactor kinetic energy for impacts at velocities above a threshold velocity.
4. Changing the mass of the blunt-ended impactor does not appear to change the threshold velocity. It does, however, appear to change the slope of the curve of delaminated area versus kinetic energy, although not enough that results are available to support definite quantitative conclusions on this point.
5. Changing the fiber weight percent and/or fiber strength changes the threshold velocity for delamination but not the appearance of the delamination patterns.
6. For the blast loaded plates, the delaminations were initiated at the boundaries, and the total delaminated area appears to be a linear function of the estimated unrecovered work.
7. In most of the plates tested by either central impact or by blast loading the principal elastic deformation mode before delamination occurs appears to be a flexural wave.
8. The DEPROP code option used, based on classical elastic laminated plate theory for orthotropic laminae, appears

to be a useful first-order tool for calculating the interlaminar shear stresses before delamination in dynamically loaded composite plates.

9. The initiation of delamination on the tension side in flexure under static loading or blast loading cannot be fully accounted for by analysis based on the reported unequal values of tension and compression moduli.

REFERENCES

1. Leeds, M.A., Schwartz, S., Holm, G. J., Krainess, A.M., Wykes, D.M., Delzell, M.T., Weazie, W.H., "NASA Technology Utilization Survey on Composite Materials," NASA-CR-129989, May 1972.
2. Gupta, B.P. and Davids, N., "Penetration Experiments with Fiberglass-Reinforced Plastics," Experimental Mechanics, Vol. 6, 1966, pp. 445-450.
3. Wrzesien, A., "Improving the Impact Resistance of Glass-Fibre Composites," Composites Vol. 3, 1972, pp. 172-174.
4. Ross, C.A. and Sierakowski, R. L., "Studies on the Impact Resistance of Composite Plates," Composites, Vol. 4, 1973, pp. 157-161.
5. Cristescu, N., Malvern, L.E. and Sierakowski, R.L., "Failure Mechanisms in Composite Plates Impacted by Blunt-Ended Penetrators," ASTM STP 568, pp. 159-172, 1975.
6. Askins, D.R. and Schwartz, H.S., "Mechanical Behavior of Reinforced Plastic Backing Materials for Composite Armor," AFML-TR-71-283, Feb., 1972.
7. Francis, P.H., Nagy, A., Pennick, H.G. and Calvit, H.H., "Ballistic Penetration Effects on Biaxially Loaded Graphite/Epoxy Composite Panels," BRL Contract Rept. No. 148, April, 1974.
8. deRosset, W.S., "Flexure Fracture of Graphite-Epoxy," BRL Memorandum Report No. 2504, July, 1975.
9. Hearle, J.W.S. and Sulton, M.A.I., "Research on a Basic Study of the High-Speed Penetration Dynamics of Textile Materials," ERO-USA TR Contract No: DATA 37-73-C-3723, May, 1974.
10. Yeung, P. and Broutman, T.J., "The Effect of Glass-Resin Interface Strength on the Impact Strength of Fiber Reinforced Plastics," To be presented at the 1977 SPI Meeting, Feb. 1977.
11. Chamis, C.C., Hanson, M.P. and Serafini, T.T., "Composite Materials: Testing and Design," ASTM STP 497, pp. 324-349, 1972.
12. Broutman, L.J. and Rotem, A., "Impact Strength and Toughness of Fiber Composite Materials," ASTM STP 568, pp. 114-133, 1975.
13. Yew, C.H. and Benedict, B.K., "Fracture of Fiber-Reinforced Beams due to Impact Loading," BRL Contract Rept. No. 212, March, 1975.

14. Beaumont, P.W.R., Reiwald, P.G., and Zweben, C., "Methods for Improving the Impact Resistance of Composite Materials," ASTM STP 568, pp. 134-158, 1975.
15. Sierakowski, R.L., Malvern, L.E., Ross, C.A., and Strickland, W.S., "Failure of Composite Plates Subjected to Dynamic Loads," Proceedings of Army Symposium on Solid Mechanics, 1976, pp.9-25, Sept. 1976.
16. Cristescu, N., Sierakowski, R.L., and Ross, C.A., "Fiber Pull Out and Delamination Processes in Composite Materials," Proceedings Society of Engineering Science (11th Annual Meeting) Duke University, Durham, North Carolina, November 11-13, 1974.
17. Ross, C.A. and Sierakowski, R.L., "Delamination Studies of Impacted Composite Plates," 46th Shock and Vibration Symposium, San Diego, California, Oct. 21-23, 1975.
18. Ross, C.A., Cristescu, N. and Sierakowski, R.L., "Experimental Studies on Failure Mechanisms of Impacted Composite Plates," Fibre Science and Technology, Vol. 9, pp. 117-188, 1976.
19. Sierakowski, R.L., Malvern, L.E. and Ross, C.A., "Dynamic Failure Modes in Impacted Composite Plates," 105th AIME Annual Meeting, Las Vegas, Nevada, Feb. 22-26, 1976.
20. Muldary, P.F., "Dynamics of Elastic Plates," M.Sc. Thesis, University of Minnesota, 1975.
21. Bascom, W.D., Jones, R.L. and Timmons, C.O., "Mixed Mode Fracture of Structural Adhesives," Adhesion Science and Technology, Vol. 9B, Ed. 2. H. Leer, Plenum Press, N.Y., 1975, p. 501.
22. Ross, C.A. and Strickland, W.S., "Response of Flat Plates Subjected to Mild Impulsive Loadings," Proceedings 45th Shock and Vibration Symposium, Dayton, Ohio, October 22-24, pp. 105-116.
23. Timoshenko, S. and Woinowsky-Krieger, S., Theory of Plates and Shells, McGraw-Hill Book Co., N.Y., N.Y., 1959.
24. Ambartsumyan, S.A., Theory of Anisotropic Plates, Technomic Publishing Co., Stamford Connecticut, 1970.
25. Ashton, J.E. and Whitney, J.M., Theory of Laminated Plates, Technomic Publishing Co., Stamford, Conn., 1970.
26. Mente, L.J. and Lee, W.N., "DEPROP-A Digital Computer Program for Predicting Dynamic Elastic-Plastic Response of Panels to Blast Loadings." AFATL-TR-76-71 Air Force Armament Laboratory, Eglin AFB, Fl.

27. Sendeckyj, G.P., "Effect of Void Content on the Behavior of Advanced Fiber Reinforced Composite Materials," Proceedings Army Symposium on Solid Mechanics, Composite Materials: The Influence of Mechanics of Failure on Design, AMMRC MS 76-3 Cape Cod, Massachusetts, Sept. 14-16, 1976
28. Jones, Robert M., Mechanics of Composite Materials, Scripta Book Co., Washington, D.C. and McGraw-Hill Book Co., New York, 1975.
29. Jones, Robert M., "Apparent Flexural Modulus and Strength of Multimodulus Materials," Journal of Composite Materials, Vol. 10, October 1976, pp 342-354.

REPORT DOCUMENTATION PAGE		READ INSTRUCTIONS BEFORE COMPLETING FORM
1. REPORT NUMBER	2. GOVT ACCESSION NO.	3. RECIPIENT'S CATALOG NUMBER
4. TITLE (and Subtitle)		5. TYPE OF REPORT & PERIOD COVERED
(6) Studies on the Penetration Mechanics of Composite Plates.		Final Jan 73 - Dec 76
7. AUTHOR(s)		6. PERFORMING ORG. REPORT NUMBER
(10) R. L. Sierakowski, L. E. Malvern C. A. Ross, N. Cristescu		(15) DAAG 29-76-G-0085
9. PERFORMING ORGANIZATION NAME AND ADDRESS		8. CONTRACT OR GRANT NUMBER(s)
Department of Engineering Sciences University of Florida Gainesville, Florida 32611		(18) ARC
11. CONTROLLING OFFICE NAME AND ADDRESS		10. PROGRAM ELEMENT, PROJECT, TASK AREA & WORK UNIT NUMBERS
(11)		(19) 11946, 5-E P - 11496 - E
14. MONITORING AGENCY NAME & ADDRESS (if different from Controlling Office)		12. REPORT DATE
U. S. Army Research Office Box CM, Duke Station Durham, North Carolina 27706		Dec 76
15. SECURITY CLASS. (of this report)		13. NUMBER OF PAGES
Unclassified		
16. DISTRIBUTION STATEMENT (of this Report)		15a. DECLASSIFICATION/DOWNGRADING SCHEDULE
Approved for public release; distribution unlimited		(12) 48p.
17. DISTRIBUTION STATEMENT (of the abstract entered in Block 20, if different from Report)		
(9) Final rept. Jan 73-Dec 76,		
18. SUPPLEMENTARY NOTES		
19. KEY WORDS (Continue on reverse side if necessary and identify by block number)		
Solid Mechanics Energy Absorption Ballistic Impact Dynamic Fracture Blast Loads Beams Composites Plates		
20. ABSTRACT (Continue on reverse side if necessary and identify by block number)		
Experimental studies have been conducted on a large number of orthotropic composite plates of 0°-90° fiber orientation subjected to kinetic energy impactors and blast type loadings. The fiberglass-epoxy composites were tested at loadings below that required to cause penetration or complete failure. A systematic study of the resultant failure patterns is reported on and a proposed model for explaining the observed plate failure presented. Some quantitative measures of plate performance under dynamic loads are indicated.		